Published April 4, 2011

A presynaptic endosomal trafficking pathway controls synaptic growth signaling

Avital A. Rodal,[1,2] Aline D. Blunk,[1,2] Yulia Akbergenova,[1,2] Ramon A. Jorquera,[1,2] Lauren K. Buhl,[1,2] and J. Troy Littleton[1,2]

[1]Department of Biology and [2]Department of Brain and Cognitive Sciences, The Picower Institute for Learning and Memory, Massachusetts Institute of Technology, Cambridge, MA 02139

Structural remodeling of synapses in response to growth signals leads to long-lasting alterations in neuronal function in many systems. Synaptic growth factor receptors alter their signaling properties during transit through the endocytic pathway, but the mechanisms controlling cargo traffic between endocytic compartments remain unclear. Nwk (Nervous Wreck) is a presynaptic F-BAR/SH3 protein that regulates synaptic growth signaling in *Drosophila melanogaster*. In this paper, we show that Nwk acts through a physical interaction with sorting nexin 16 (SNX16). SNX16 promotes synaptic growth signaling by activated bone morphogenic protein receptors, and live imaging in neurons reveals that SNX16-positive early endosomes undergo transient interactions with Nwk-containing recycling endosomes. We identify an alternative signal termination pathway in the absence of *Snx16* that is controlled by endosomal sorting complex required for transport (ESCRT)–mediated internalization of receptors into the endosomal lumen. Our results define a presynaptic trafficking pathway mediated by SNX16, NWK, and the ESCRT complex that functions to control synaptic growth signaling at the interface between endosomal compartments.

Introduction

Growth factor signaling in neurons controls the expansion of synaptic arbors in response to activity and external stimuli, leading to long-lasting changes in synapse strength and connectivity that underlie learning and memory. Receptor complexes regulating growth factor signal transduction are internalized via endocytosis and directed to specific subcellular membrane compartments from which they exhibit distinct signaling properties, caused by compartment-specific posttranslational modifications and degradative events, or interactions with local binding partners (Sadowski et al., 2009). Therefore, defining the mechanisms by which the rate and direction of the flow of endosomal protein traffic are controlled is critical to determining how neuronal signal transduction pathways are tuned up and down after activation. A host of protein factors control membrane traffic through the interconnected tubules and vesicles of the endosomal system, and sorting occurs by isolation of cargo in membrane domains of defined geometry and lipid composition (Bonifacino and Rojas, 2006). Proteins modulating membrane dynamics and organization are thus well positioned to control the sorting and activities of signaling complexes during endosomal processing.

The *Drosophila melanogaster* larval neuromuscular junction (NMJ) serves as a useful model for the regulation of synaptic growth signaling as the muscle surface area expands 100-fold over 4 d of larval development, requiring increased input from its innervating motor neuron to drive contraction. NMJ synaptic arbors expand by adding matched pre- and postsynaptic specializations (termed synaptic boutons) in response to motor neuron synaptic activity, retrograde signals from the muscle to the neuron, and anterograde signals from the neuron to the muscle (Packard et al., 2002; McCabe et al., 2003; Yoshihara et al., 2005). Mutants in proteins regulating endocytosis fail to properly

Correspondence to Avital A. Rodal: arodal@brandeis.edu

A.A. Rodal's present address is Brandeis University, Waltham, MA 02454.

Abbreviations used in this paper: Arp2/3, actin-related protein 2/3; BMP, bone morphogenic protein; Cpx, complexin; EPSC, excitatory postsynaptic current; ESCRT, endosomal sorting complex required for transport; IB, immunoblot; IHC, immunohistochemistry; mRFP, monomeric RFP; MVB, multivesicular body; NMJ, neuromuscular junction; PCC, Pearson's correlation coefficient; PX, Phox homology; SH3, Src homology 3; SNX16, sorting nexin 16; UAS, upstream activating sequence; WASp, Wiskott–Aldrich syndrome protein; Wg, Wingless.

Supplemental Material can be found at:
http://jcb.rupress.org/content/suppl/2011/04/04/jcb.201009052.DC1.html
Original image data can be found at:
http://jcb-dataviewer.rupress.org/jcb/browse/3258

The Rockefeller University Press $30.00
J. Cell Biol. Vol. 193 No. 1 201–217
www.jcb.org/cgi/doi/10.1083/jcb.201009052

Published April 4, 2011

attenuate growth factor signaling at the NMJ, resulting in abnormal overgrowth of the synaptic arbor, with the hallmark phenotype of increased arbor branching and the formation of "satellite" boutons off the main axis of the axon terminal (Dickman et al., 2006). One such gene, *nwk* (*nervous wreck*), encodes a neuron-specific member of the F-BAR (Fes/CIP4 homology Bin-Amphiphysin-Rvs)/SH3 (Src homology 3) family of lipid-binding proteins that control the force-generating assembly of actin filaments at endosomal compartments by activating WASp (Wiskott–Aldrich syndrome protein)/Arp2/3 (actin-related protein 2/3)-mediated actin polymerization (Coyle et al., 2004). Nwk attenuates the retrograde BMP (bone morphogenic protein) signal mediated by Glass Bottom Boat through its presynaptic receptor Tkv (Thickveins; O'Connor-Giles et al., 2008), colocalizes with the recycling endosome marker Rab11, and functions together with the endosomal GTPase Cdc42 to control WASp/Arp2/3-mediated actin assembly (Rodal et al., 2008). However, the mechanisms by which Nwk attenuates synaptic growth factor signaling at this compartment are unknown.

Here, we describe the identification of a novel Nwk-binding partner, sorting nexin 16 (SNX16). SNX16 is a member of the sorting nexin family of proteins that regulate endosomal traffic and are defined by a phosphoinositide-binding Phox homology (PX) domain (Hanson and Hong, 2003; Choi et al., 2004; Cullen, 2008). We demonstrate that SNX16- and Nwk-containing compartments transiently interact in nerve terminals and that signaling at early endosomes is attenuated either through Nwk–SNX16 interactions or through endosomal sorting complex required for transport (ESCRT)–mediated internalization into the endosomal lumen. SNX16–Nwk-mediated traffic regulates synaptic growth signaling cascades, including the BMP and Wingless (Wg) pathways, and is specifically required to down-regulate activated receptors. Our results provide a mechanism by which protein traffic between endosomal intermediates at synapses controls the output of signal transduction pathways, leading to synaptic growth.

Results

Nwk physically interacts with SNX16

Nwk is a predicted lipid-binding protein that activates actin polymerization in vitro through WASp/Arp2/3 (Rodal et al., 2008) and, thus, may define an actin-dependent step of endocytosis critical for the down-regulation of growth factor signaling at the *Drosophila* NMJ. However, the specific mechanism by which it acts is unclear. To elucidate the function of Nwk in membrane traffic, we conducted a yeast two-hybrid screen using full-length Nwk as bait and identified a carboxy-terminal fragment (aa 236–407) of the *Drosophila CG6410* gene product as an Nwk-interacting protein. We named this gene *Snx16*, as it encodes the single *Drosophila* homologue of the mammalian protein SNX16, which is involved in membrane traffic at endosomal compartments (Hanson and Hong, 2003; Choi et al., 2004). SNX16 homologues are found in animals ranging from insects to mammals (Fig. S1), but neither *Snx16* nor *nwk* is recognizable in *Caenorhabditis elegans*. *Drosophila* SNX16 consists of a poorly conserved amino-terminal region, a highly conserved PX domain (which is predicted to bind to phosphoinositides), and a conserved carboxy-terminal coiled-coil domain.

To define the domains of Nwk and SNX16 that are required for their interaction, we generated a series of deletion constructs and assayed their ability to interact in the yeast two-hybrid assay (Fig. 1 A). SNX16–Nwk interactions required a region of the SNX16 coiled-coil domain near the PX domain (aa 346–363). Three glutamate residues in this region are highly conserved in all examined Snx16 homologues (Fig. 1 B), and mutation of these three glutamates to alanine (E347A, E350A, and E351A, hereafter referred to as SNX16^{3A}) abolished yeast two-hybrid interactions between full-length Nwk and SNX16 (aa 246–407). The SNX16-binding site on Nwk mapped to aa 637–700, encompassing the second SH3 domain. However, the mutation W677A, which disrupts the ability of this SH3 domain to bind to proline-rich targets (Rodal et al., 2008), did not abolish the Nwk–SNX16 interaction, suggesting that binding is not mediated by canonical interactions of the SH3 domain.

To validate the Nwk–SNX16 interaction observed in the yeast two-hybrid assay, we conducted GST pull-down assays from *Drosophila* head extracts. GST-SNX16 (aa 335–407; coiled coil domain) precipitated endogenous Nwk from *Drosophila* head extracts (Fig. 1 C). Endogenous SNX16 is expressed at low levels and was difficult to detect with our antibodies; therefore, we overexpressed SNX16 or SNX16-GFP using the GAL4/upstream activating sequence (UAS) system (Brand and Perrimon, 1993) and the panneuronal GAL4 driver *elav*^{C155} and evaluated the ability of this overexpressed protein to associate with Nwk in *Drosophila* head extracts. SNX16 and SNX16-GFP each associated specifically with GST-Nwk (aa 1−731) but not GST alone (Fig. 1 D). In addition, GST-Nwk (aa 1–731) coprecipitated with recombinant SNX16 (aa 220–407; PX and coiled-coil domain) from *Escherichia coli* extracts but only poorly with SNX16^{3A} (aa 220–407; Fig. 1 E). As we were unable to detect an association of endogenous SNX16 with Nwk by coimmunoprecipitation (unpublished data) and only a small proportion of SNX16 or Nwk in extracts precipitated with its reciprocal GST-tagged binding partner, we hypothesize that the interaction between Nwk and SNX16 is transient and likely regulated by additional protein- or lipid-binding partners.

SNX16 localizes to early endosomes

Mammalian SNX16 promotes the traffic of growth factor receptors from early to late endosomes (Hanson and Hong, 2003; Choi et al., 2004). To determine the cellular compartment in which *Drosophila* SNX16 acts, we first localized SNX16 in cultured *Drosophila* cells. SNX16-GFP and SNX16-mCherry localized to the perimeter of intracellular structures that were distributed throughout the cell interior but excluded from the nucleus (Fig. 2, A and B). Localization of SNX16-GFP to these structures was severely reduced upon treatment with wortmannin, a phosphatidylinositol 3-kinase inhibitor, which is consistent with the predicted affinity of the SNX16 PX domain for phosphatidylinositol 3-phosphate and suggests that the PX domain is critical for SNX16 association with endomembranes (Fig. 2 A). We cotransfected cells with SNX16-mCherry or SNX16^{3A}-mCherry and tagged markers of early endosomes

Published April 4, 2011

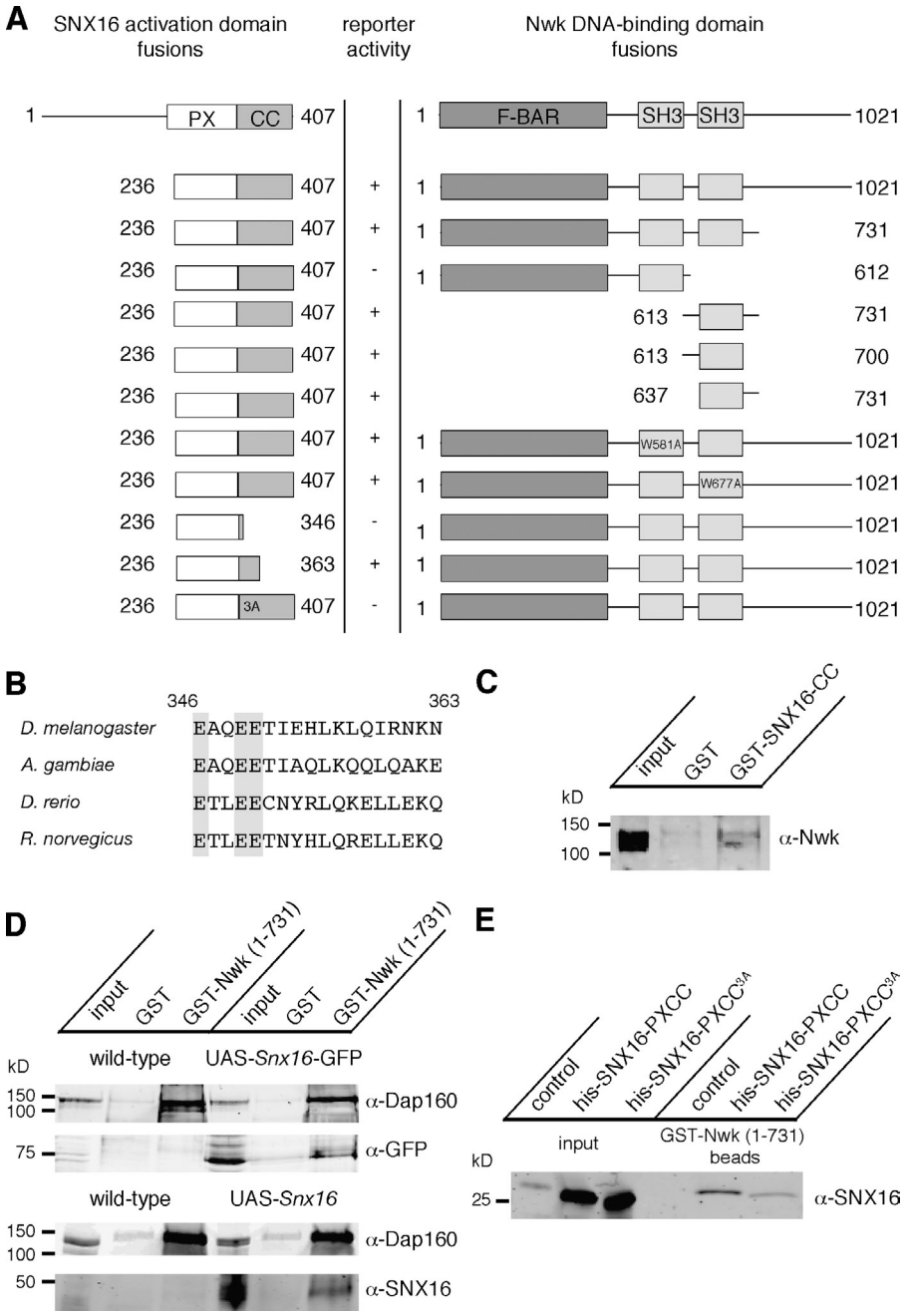

Figure 1. **SNX16 physically interacts with Nwk.** (A) Schematic of Nwk and SNX16 domain organization and summary of yeast two-hybrid interactions. (B) Alignment of SNX16 homologues between aa 346 and 363 of *Drosophila* SNX16. NCBI Protein database accession numbers and a full SNX16 alignment are shown in Fig. S1. Shaded glutamate residues are required for Nwk–Snx16 interactions. (C) GST and GST-SNX16 (aa 335–407; coiled coil [CC]) were used to precipitate binding partners from wild-type *Drosophila* head extracts. Equal amounts of precipitates were immunoblotted with α-Nwk antibodies. The first lane represents 2.5% of the input compared with experimental samples. (D) GST and GST-Nwk (aa 1–731) were used to precipitate binding partners from wild-type, UAS-*Snx16*, and UAS-*Snx16*-GFP–expressing *Drosophila* head extracts. Equal amounts of precipitates were immunoblotted with α-GFP, α-SNX16, or α-Dap160 antibodies. Dap160 has previously been shown to interact with Nwk (O'Connor-Giles et al., 2008; Rodal et al., 2008). The first and fourth lanes represent 2% of the input compared with experimental samples. (E) GST-Nwk (aa 1–731) was coexpressed in *E. coli* with empty vector, SNX16 (aa 220–407; PX and coiled-coil domains), or SNX16^{3A} (aa 220–407), precipitated on glutathione agarose, and immunoblotted with α-SNX16 antibodies. *A. gambiae*, *Anopheles gambiae*; *D. rerio*, *Danio rerio*; *R. norvegicus*, *Rattus norvegicus*.

(GFP-Rab5) and recycling endosomes (GFP-Rab11) and spread them on concanavalin A for a better resolution of internal structures (Rogers et al., 2003). SNX16 colocalized with a subset of Rab5-positive structures (Pearson's correlation coefficient [PCC] of 0.41 ± 0.11, $n = 4$) but only poorly with Rab11 (PCC of 0.11 ± 0.01, $n = 5$; Fig. 2 B). SNX16^{3A}-mCherry localization was similar to SNX16-mCherry (Fig. 2 B). We then transfected *Drosophila* cells with the human transferrin receptor and assessed endocytic uptake of its labeled ligand, transferrin. Transferrin was not recycled back to the cell surface in these cells, as has previously been shown in similar cell types (Van Hoof et al., 2005), but instead accumulated in an intracellular compartment labeled by Rab5 and SNX16 but not Rab11 (PCC of 0.64 vs. 0.45; Fig. 2 C). We conclude that SNX16 resides in an early endosomal compartment that is a functional site of receptor-mediated endocytosis. Finally, we expressed Nwk-GFP in cultured cells. Although other F-BAR proteins induce massive lipid tubulation when expressed in cultured cells (Frost et al., 2009), Nwk localization was primarily cytoplasmic, with occasional faint intracellular puncta. When SNX16–monomeric RFP (mRFP) was coexpressed in these cells, we observed that Nwk-GFP structures overlapped with a small subset of SNX16 puncta (PCC of 0.83 ± 0.01, $n = 5$; Fig. 2 D). Thus, Nwk and SNX16 partially colocalize in heterologous cells.

We next localized SNX16 at the *Drosophila* NMJ using the panneuronal GAL4 driver *elav*^{C155}, as we were unable to detect endogenous Snx16 in embryos or larvae using our antisera (Fig. S2). Both SNX16 and SNX16-GFP localized to several

Published April 4, 2011

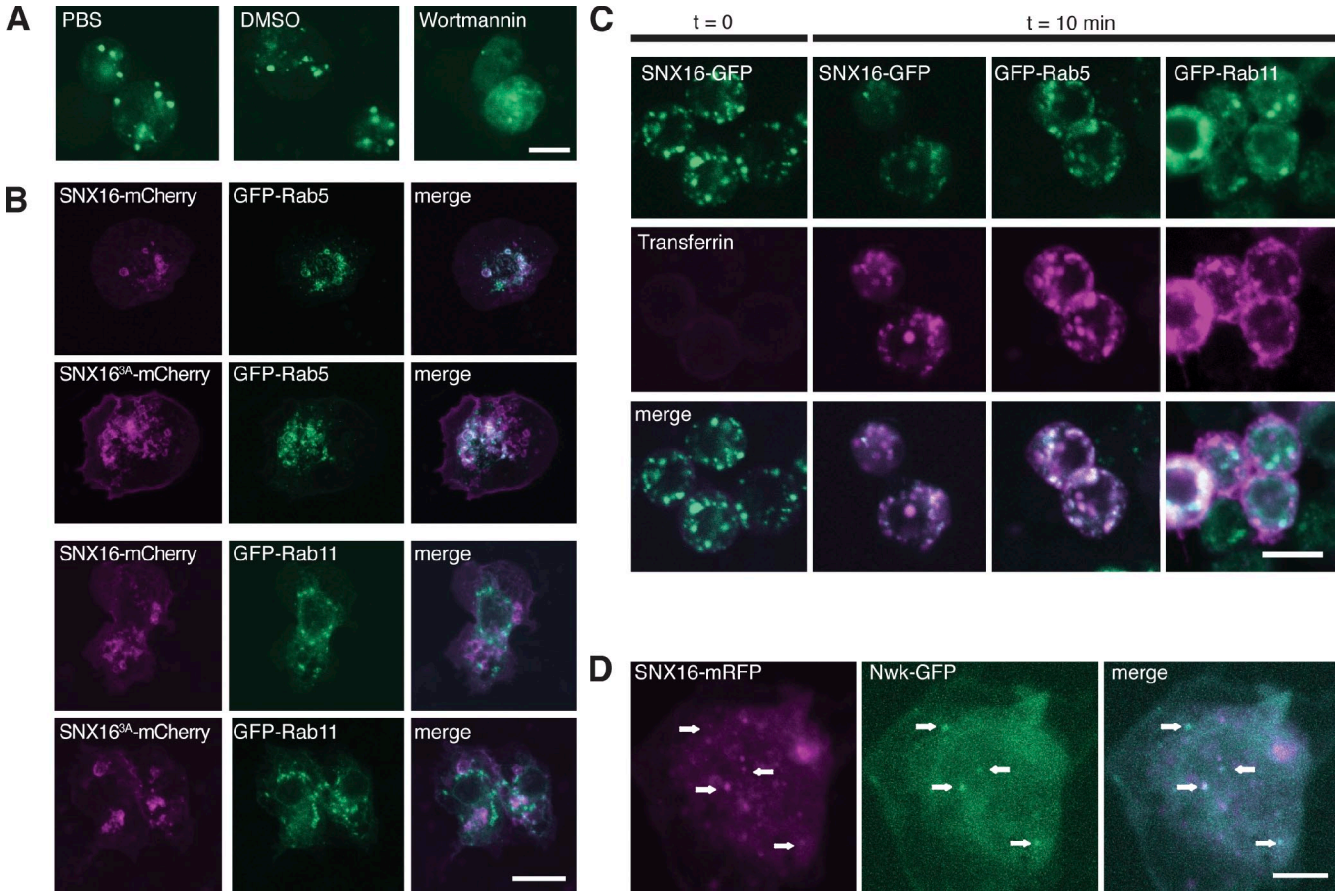

Figure 2. **SNX16 localizes to Rab5-positive early endosomes.** (A) Kc167 cells transfected with *Snx16*-GFP were treated with wortmannin and then fixed and imaged by confocal microscopy. Single confocal sections are shown. (B) S2 cells transfected with the indicated constructs were spread on concanavalin A, fixed, and imaged. 2D projections of confocal stacks are shown. (C) Kc167 cells transfected with human transferrin receptor and the indicated constructs were incubated with Alexa Fluor 546–labeled transferrin for the indicated times and then fixed and imaged. Single confocal sections are shown. (D) Nwk localizes to a subset of SNX16 puncta. S2 cells were transfected with *Snx16*-mRFP and *nwk*-GFP and spread on concanavalin A before fixation and imaging. A 2D projection of a confocal stack is shown. Arrows indicate overlapping puncta. Bars, 10 µm.

bright puncta in each synaptic bouton, which overlapped well with the early endosomal markers Rab5 and Rab4 (Fig. 3, A and B) but not the recycling endosome marker Rab11 (Fig. 3 C). 80.9 ± 8.6% of SNX16 puncta per NMJ overlapped with Rab5 puncta (n = 5 NMJs), and 77.2 ± 15.1% of SNX16 puncta per NMJ overlapped with Rab4 puncta (n = 4 NMJs). It has previously been reported that the BMP receptor Tkv, which is misregulated in *nwk* mutants (O'Connor-Giles et al., 2008), resides in Rab5-positive endosomal structures at the NMJ (Wang et al., 2007), and we found that SNX16 puncta colocalized with Tkv-GFP (35.3 ± 10.2% of SNX16 puncta overlapped with Tkv-GFP puncta; n = 5 NMJs; Fig. 3 D). SNX16-GFP also colocalized with the presynaptic portion of Hrs (Lloyd et al., 2002), a component of the ESCRT complex that drives internalization of cargo into the endosomal lumen (Fig. 3 E). 49.4 ± 3.7% of SNX16-GFP puncta overlapped with Hrs puncta (n = 5 NMJs, note that Hrs is predominantly postsynaptic with a more minor presynaptic component [Lloyd et al., 2002] and that only this fraction of presynaptic Hrs puncta contain neuronally expressed SNX16). Finally, immunoelectron microscopy with anti-GFP antibodies detected both SNX16-GFP and SNX16^{3A}-GFP on the outside surface of ∼200-nm diameter compartments at the NMJ (Fig. 3 F), in which internal vesicles could sometimes be seen. Thus, we conclude that SNX16 localizes primarily to early endosomes and multivesicular bodies (MVBs), which are sites of receptor traffic at the *Drosophila* larval NMJ.

Nwk localizes to a novel compartment that transiently interacts with SNX16 endosomes at the NMJ

In fixed tissue, Nwk localizes to a synaptic subdomain termed the "periactive zone" (Roos and Kelly, 1999; Sone et al., 2000) that closely surrounds sites of synaptic vesicle release. SNX16-GFP puncta localized within or adjacent to Nwk-positive periactive zones in fixed NMJs, but it was difficult to infer the nature of their functional relationship from this localization. We reasoned that analysis of the dynamic localization of SNX16 and Nwk relative to each other would provide more information about their relationship. Panneuronally expressed Nwk-mRFP (Fig. 4 A; previously described in O'Connor-Giles et al., 2008) rescues the temperature-sensitive seizure phenotype of *nwk* mutant adult *Drosophila* (not depicted), suggesting that it encodes a functional protein. In contrast to the periactive zone localization of either endogenous or overexpressed α-Nwk

Published April 4, 2011

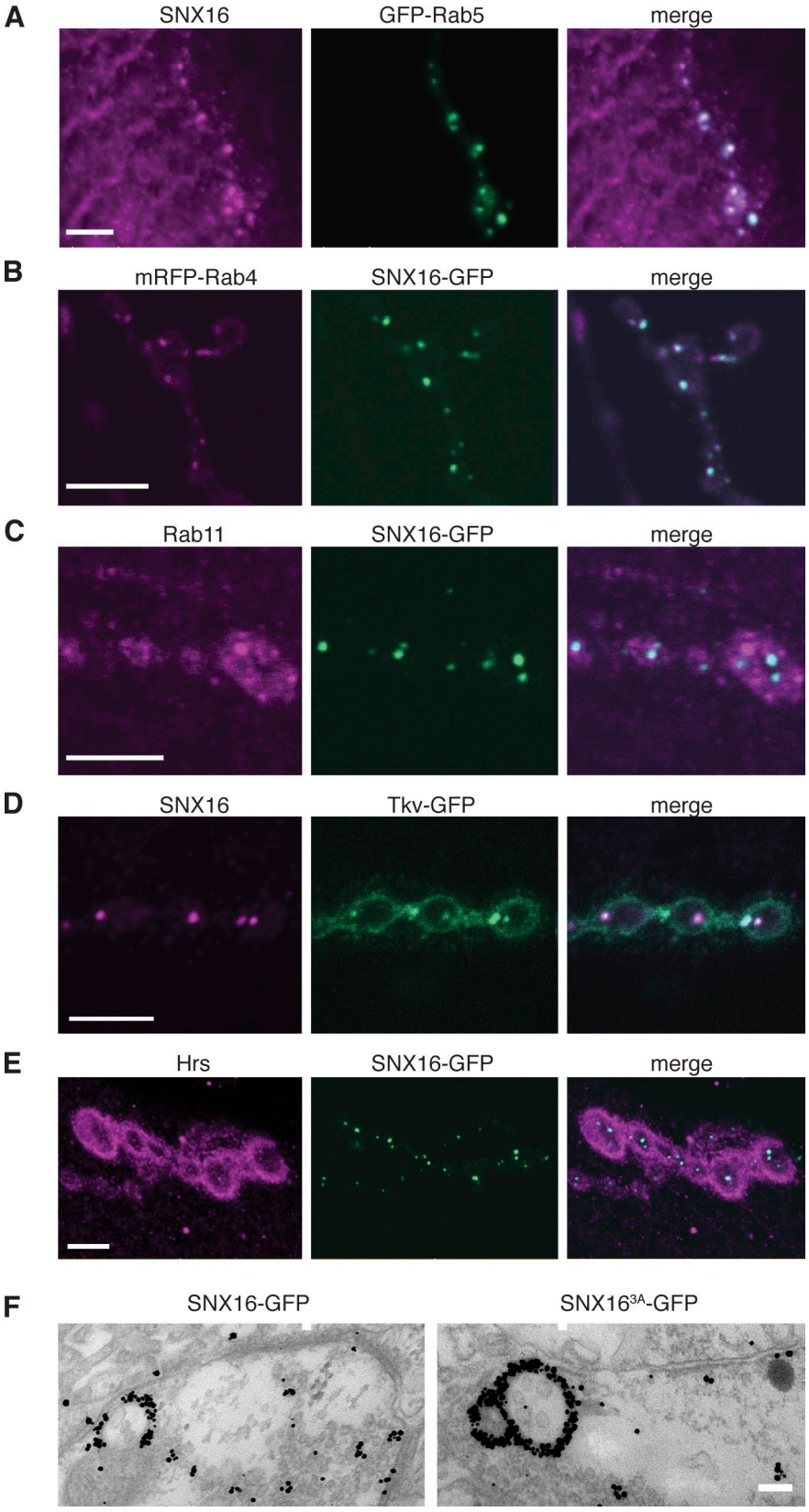

Figure 3. **Localization of SNX16 to endosomes at the *Drosophila* NMJ.** (A) *elav*^{C155}; UAS-*Snx16*;UAS-GFP-*Rab5* larvae stained with α-SNX16 antibodies. (B) *elav*^{C155};UAS-*Snx16*-GFP;UAS-mRFP-*Rab4* larvae. (C) *elav*^{C155};UAS-*Snx16*-GFP larvae stained with α-Rab11 antibodies. (D) *elav*^{C155};UAS-*Snx16*;UAS-*tkv*-GFP larvae stained with α-SNX16 antibodies. (E) *elav*^{C155};UAS-*Snx16*-GFP larvae stained with α-Hrs antibodies (also available in the JCB DataViewer). (F) *elav*^{C155};UAS-*Snx16*-GFP and UAS-*Snx16*^{3A}-GFP larvae stained with α-GFP antibodies and processed for immunoelectron microscopy. Bars: (A–E) 5 µm; (F) 100 nm.

immunoreactivity in fixed tissue (Coyle et al., 2004; Rodal et al., 2008), Nwk-mRFP localized diffusely in live nerve terminals, with several bright puncta per NMJ (2.6 ± 0.5 particles/NMJ on muscle 6/7 in segments A2 and A3, $n = 5$ NMJs; Fig. 4 B). However, when these samples were fixed and extracted with detergents for antibody staining, mRFP fluorescence collapsed toward more defined structures in each bouton similar to endogenous or overexpressed untagged Nwk, and bright puncta were

Published April 4, 2011

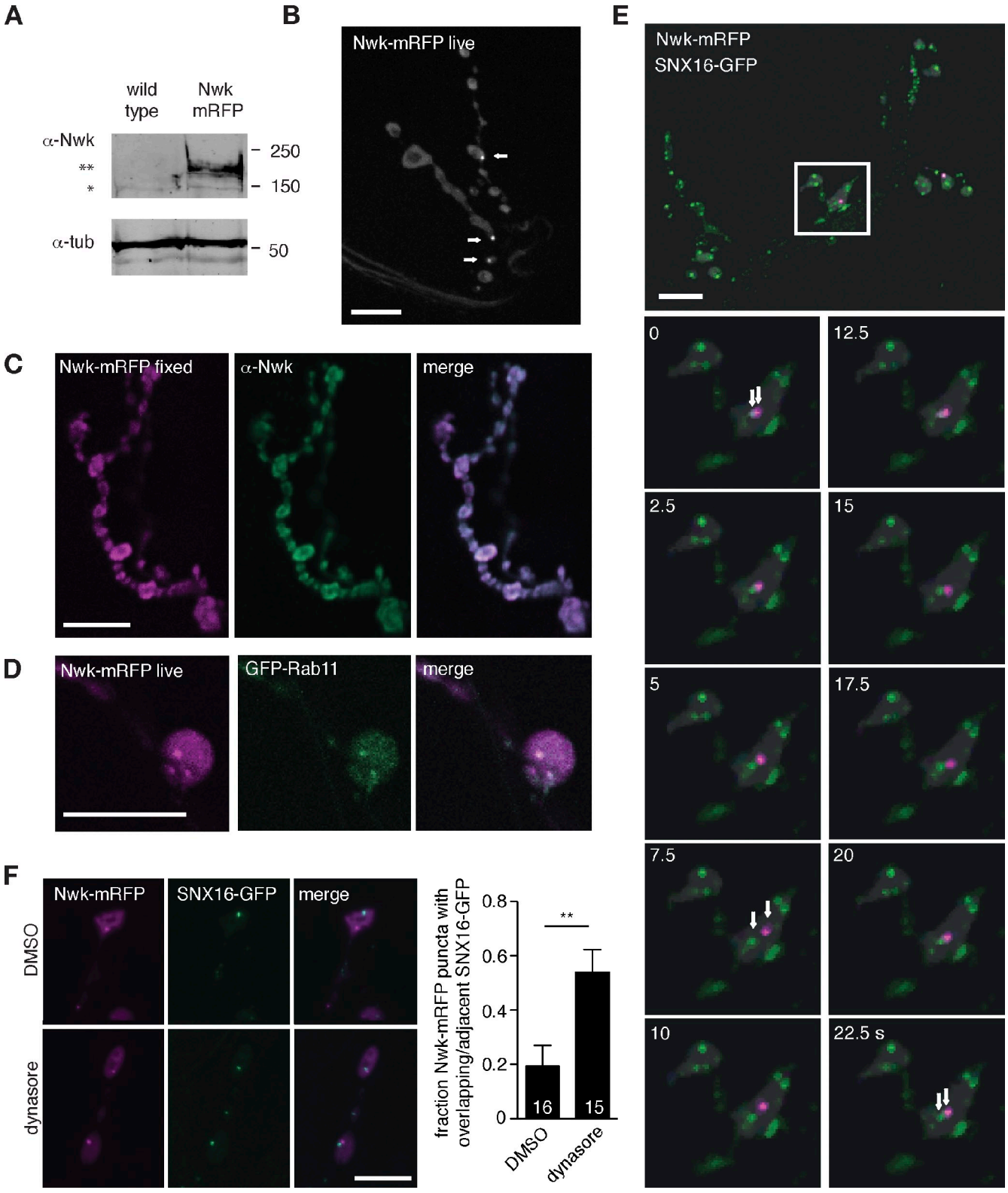

Figure 4. **Nwk in live NMJs localizes to puncta that transiently interact with SNX16 endosomes.** (A) *elav*^{C155};Nwk-mRFP expression in α-Nwk IBs of *Drosophila* larval fillet extracts. The single asterisk indicates endogenous Nwk; the double asterisk indicates Nwk-mRFP. Molecular masses are given in kilodaltons. tub, tubulin. (B) Localization of Nwk-mRFP in live third instar NMJs. Arrows indicate Nwk-mRFP puncta. (C) Localization of Nwk-mRFP in fixed third instar NMJs. Nwk collapses to discrete structures upon fixation, and Nwk puncta are not strongly detected by α-Nwk antibodies. (D) Nwk-mRFP puncta colocalize with GFP-Rab11 at NMJs. (E) Localization of Nwk-mRFP and SNX16-GFP in live third instar larval NMJs. Time-lapse recordings of these NMJs are shown in Videos 1, 2, and 3. The white box indicates the area shown in the time-lapse images below. Arrows track a pair of Nwk-mRFP and SNX16-GFP puncta. (F) The dynamin inhibitor dynasore drives association of Nwk and SNX16 particles. The quantification shows the mean fraction of Nwk particles with a SNX16 particle within 1 µm of their center. Error bars are means ± SEM, and the number of samples averaged in each measurement is indicated at the base of each bar. **, $P < 0.01$. Bars, 10 µm.

Published April 4, 2011

difficult to distinguish in or near these structures (Fig. 4 C). Because we had not previously identified these Nwk puncta in fixed tissue, we stained fixed extracted Nwk-mRFP larvae with anti-Nwk and anti-mRFP antibodies (Fig. 4 C and not depicted). Neither antibody recognized Nwk-mRFP puncta in fixed extracted tissue, suggesting that the Nwk puncta are in a structure that is poorly accessible to antibodies and disrupted upon detergent extraction. These results suggest that the previously described periactive zone localization of Nwk is likely triggered by fixation and extraction and that the diffuse and occasionally punctate localization of Nwk-mRFP observed in live tissue reflects a physiologically relevant pattern.

To further understand the nature of the Nwk compartment, we colocalized Nwk-mRFP with GFP-Rab11. Nwk and Rab11 colocalize in fixed cells (Rodal et al., 2008), and Rab11 is a marker of the recycling endosome. GFP-Rab11 exhibited a very similar pattern in live NMJs to Nwk-mRFP (largely diffuse with occasional puncta), and many GFP-Rab11 puncta colocalized (Fig. 4 D) and moved together (not depicted) with Nwk-mRFP puncta. Thus, the Nwk compartment has features of a recycling endosome, which in diverse cell types, acts to recycle endocytosed cargo from early endosomes to the plasma membrane.

We imaged the dynamics of Nwk and SNX16 compartments using spinning-disk confocal microscopy to rapidly record their positions. Nwk-mRFP and SNX16-GFP particles moved within synaptic boutons with no apparent directionality. Nwk puncta made frequent contact with SNX16 puncta, and sometimes Nwk and SNX16 puncta translocated together within the bouton for several seconds and then separated (Fig. 4 E and Videos 1, 2, and 3). In each NMJ, Nwk particles contacted SNX16 particles a mean of 1.2 ± 0.40 times/min or 0.78 ± 0.45 times/min/Nwk particle (n = 14 particles in five NMJs). These results suggest that Nwk and SNX16 exist in independent compartments that transiently interact, perhaps leading to an exchange of cargo.

Transfer of cargo-containing membranes is likely to require a scission event, and Nwk interacts with dynamin (O'Connor-Giles et al., 2008; Rodal et al., 2008), a GTPase that drives membrane scission (Mettlen et al., 2009). We therefore reasoned that acute inhibition of dynamin with the small molecule inhibitor dynasore (Macia et al., 2006) might block the transfer of membranes between SNX16 and Nwk compartments. To validate the use of dynasore in *Drosophila*, we tested whether dynasore treatment mimics the synaptic vesicle endocytosis defects in the dynamin mutant *Shibire*^{ts1}, which exhibits progressive rundown of the evoked excitatory postsynaptic currents (EPSCs) during high-frequency stimulation of the nerve (Delgado et al., 2000), whereas wild-type NMJs decline to a semisteady state that is sustained by vesicle recycling. Indeed, dynasore (but not vehicle treatment) causes a progressive rundown of EPSCs (Fig. S3). To test the role of dynamin in Nwk–SNX16 particle interactions, we treated dissected larvae with dynasore under conditions that cycle through the entire NMJ pool of dynamin (Ramaswami et al., 1994) and then fixed them without extraction for the imaging of puncta. We found that 53.9 ± 8.4% of Nwk-mRFP particles colocalized or collapsed adjacent to an SNX16-GFP particle upon treatment with dynasore (n = 59 particles in 15 NMJs; Fig. 4 F). In contrast, only 17 ± 7.6% of Nwk-mRFP particles were found colocalizing or near to an SNX16-GFP particle in control DMSO treatments (n = 35 particles in 16 NMJs; Fig. 4 F). Thus, dynamic interactions between Nwk and SNX16 particles in NMJs depend on dynamin, suggesting that their associations may lead to an exchange of membrane and/or cargo between compartments.

Nwk attenuates the growth-promoting activity of SNX16

To explore the function of SNX16 at the NMJ using genetics, we overexpressed *Snx16*-GFP and the Nwk-binding mutant *Snx16*^{3A}-GFP in the nervous system using the GAL4 driver *elav*^{C155}. Wild-type *Snx16*-GFP–overexpressing larval NMJs exhibit a small but significant increase in bouton number compared with wild-type controls (Fig. 5, A–D). However, when we overexpressed *Snx16*^{3A}-GFP, we observed a much more dramatic NMJ overgrowth phenotype with excessive branching of axon terminal arbors similar to the *nwk* mutant phenotype, with an increase in both overall bouton number and satellite bouton number (Fig. 5, A–D). We recapitulated this result with two independent transgenic insertions of *Snx16*^{3A}-GFP (Fig. 5, B–D) and verified that expression levels were similar between wild-type and mutant transgenes (not depicted).

To evaluate whether the overexpression phenotype of *Snx16*-GFP was related to its function with Nwk, we tested whether cooverexpression of Nwk could alter the synaptic overgrowth phenotype of SNX16 overexpression. Nwk overexpression on its own does not cause a synaptic growth phenotype (Fig. 5 E; O'Connor-Giles et al., 2008; Rodal et al., 2008). We found that cooverexpression of Nwk-mRFP (but not a control RFP transgene) suppresses the synaptic overgrowth phenotype resulting from overexpression of wild-type *Snx16*-GFP but notably not *Snx16*^{3A}-GFP (Fig. 5 E), suggesting that the *Snx16* phenotype results from an imbalance in specific Nwk–SNX16 physical interactions and substantiating these interactions in vivo. Finally, we tested whether BMP signaling, which is upregulated in Nwk mutants (O'Connor-Giles et al., 2008), was also increased upon overexpression of *Snx16* by measuring the levels of the Trio protein, a Rac GTPase exchange factor whose expression is directly increased by BMP signals (Ball et al., 2010). Trio protein levels were increased at the NMJ in *Snx16*-GFP and *Snx16*^{3A}-GFP–expressing larvae (Fig. 5 E). These results suggest that interactions of Snx16 with Nwk are critical for the attenuation of synaptic growth signals downstream of BMP signaling.

Two models are consistent with the synaptic overgrowth phenotype resulting from *Snx16*^{3A}-GFP overexpression. One interpretation is that Snx16 positively regulates and acts upstream of Nwk together with some additional factor, and upon overexpression of *Snx16*^{3A}-GFP, this factor is titrated away from endogenous Nwk, resulting in an *nwk* loss-of-function phenotype. The second interpretation is that *nwk* negatively regulates *Snx16*, and SNX16^{3A}-GFP is thus an overactive form of the protein that drives unregulated synaptic growth. To distinguish the order in which *nwk* and *Snx16* act, we generated loss-of-function alleles of *Snx16*. In the first model, *nwk;Snx16* double mutants

Published April 4, 2011

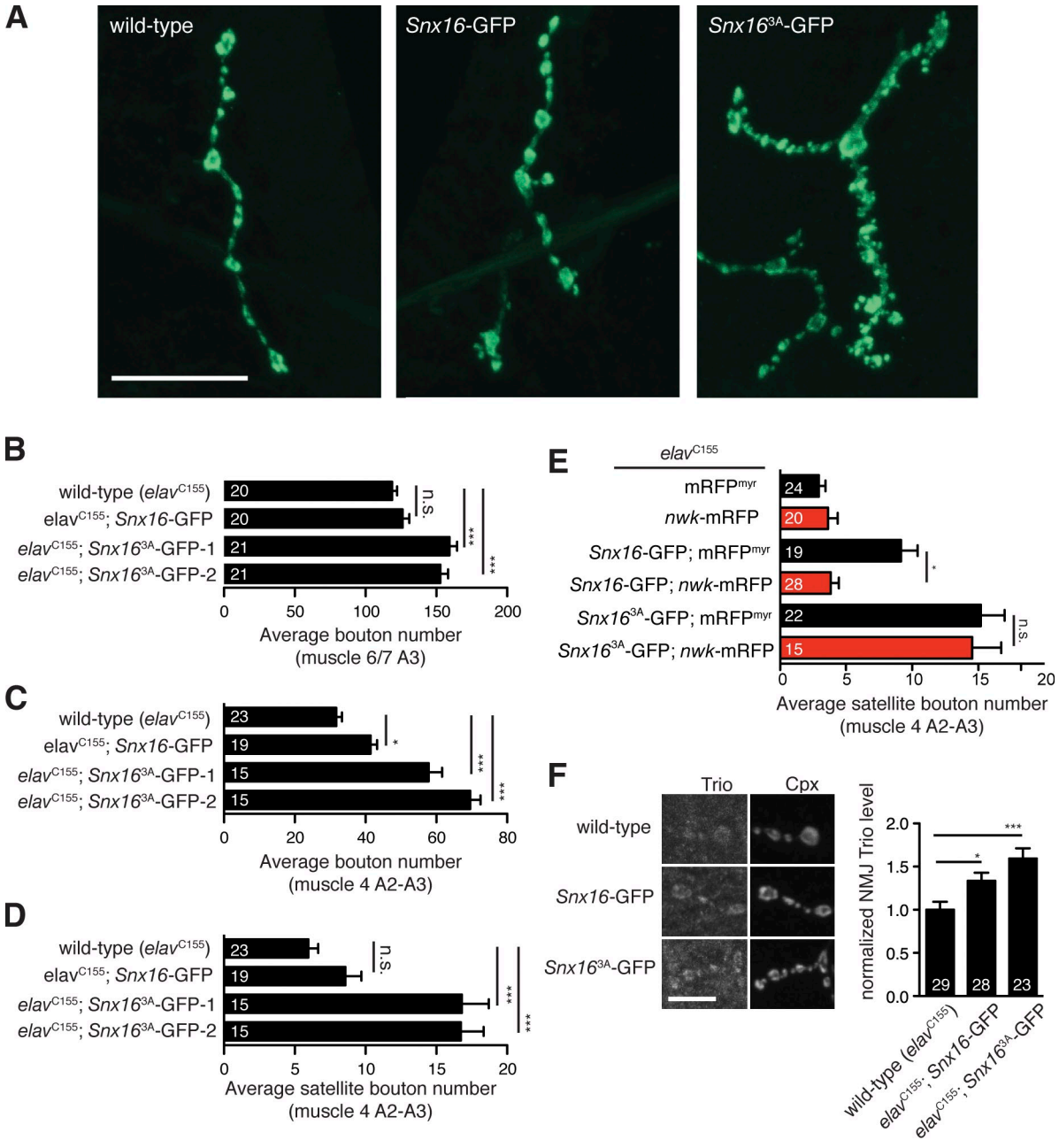

Figure 5. **A Nwk-binding mutant of Snx16 recapitulates the *nwk* phenotype.** (A) Representative confocal projections of anti-complexin (Cpx) staining from NMJs of the indicated genotype under the control of the *elav*^{C155} GAL4 driver. (B) Quantification of the mean bouton number for muscle 6/7. (C) Quantification of the mean bouton number for muscle 4. (D) Quantification of the mean satellite bouton number for muscle 4. (E) Cooverexpression of Nwk-mRFP suppresses the *Snx16* but not the *Snx16*^{3A} overexpression phenotype. Black bars indicate control animals expressing mRFP, and red bars indicate animals expressing Nwk-mRFP. (F) *Snx16*^{3A} overexpression increases BMP signaling. Trio protein levels are increased in muscle 6/7 NMJs. Error bars are means ± SEM, and the number of samples averaged in each measurement is indicated at the base of each bar. *, P < 0.05; ***, P < 0.005. Bars: (A) 20 µm; (F) 5 µm.

would be expected to phenocopy *nwk* mutants. In the second model, *nwk;Snx16* mutants would be expected to phenocopy *Snx16* mutants.

We used two complementary sources for loss-of-function alleles of *SNX16*. First, we obtained a PiggyBac transposable element insertion (PBac[RB]CG6410^{e01600}) that disrupts the coding region of *Snx16* (*Snx16*^{PB}) 366 bp downstream of the Snx16 start codon (Fig. 6 A). This allele reduces the *Snx16* transcript to 1% of the wild-type level in quantitative RT-PCR, but does not affect the adjacent gene *CG10934* (Fig. 6 B). Second, we imprecisely excised a *P* element (P[EPgy2]EY10175) inserted 51 bp 5′ of the predicted transcriptional start site of *Snx16*, resulting in the deletion of the entire *SNX16*-coding region (Fig. 6 A). Animals containing heterozygous combinations of *Snx16* mutant alleles with each other and with the 20-gene deficiency Df(2R)Exel7150 were viable and fertile. We examined NMJ morphology in these animals and found no statistically significant phenotype compared with genetically matched controls (Fig. 6, C and D), although there was a trend toward reduced synaptic growth.

Published April 4, 2011

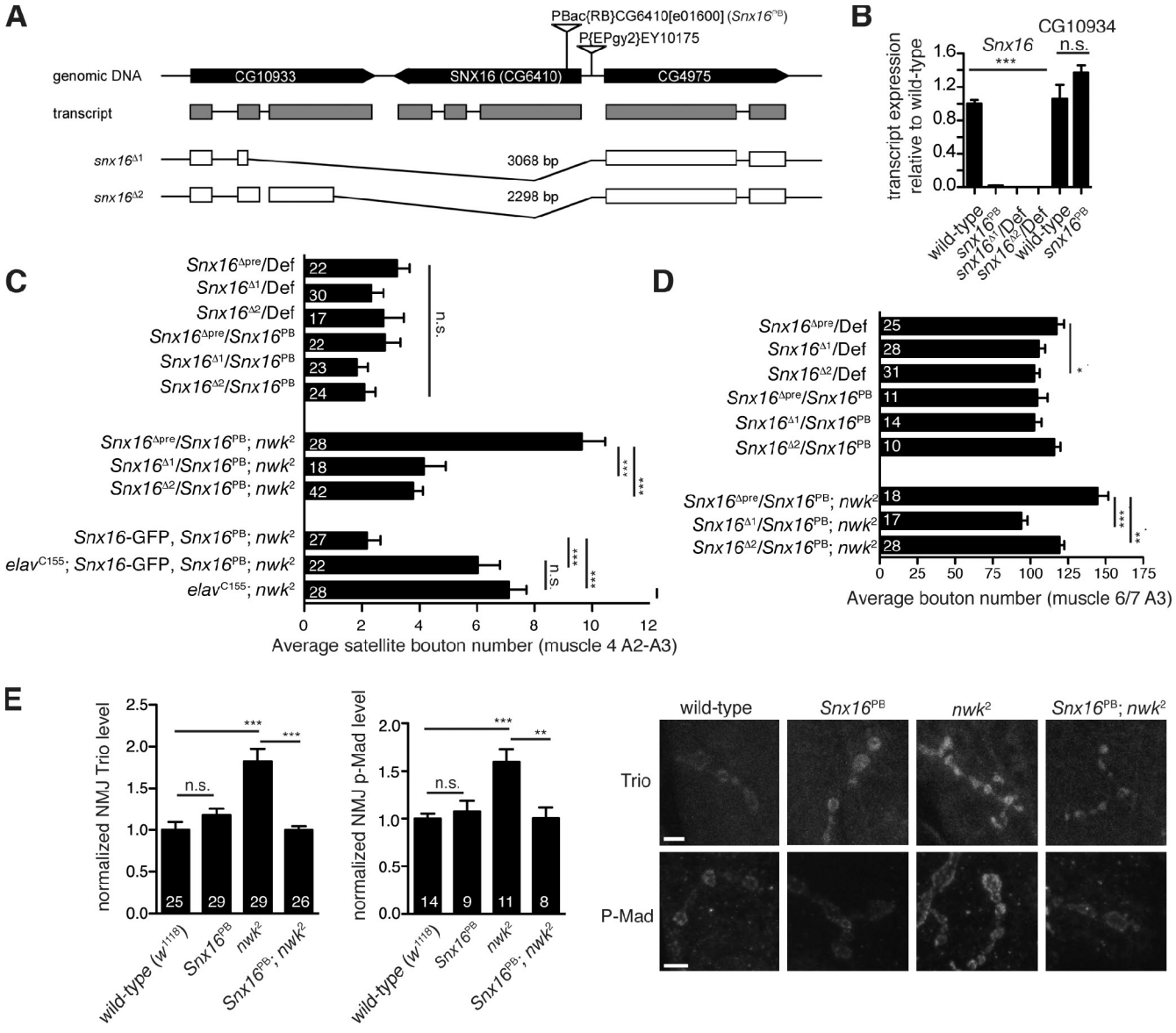

Figure 6. **Loss of *SNX16* suppresses the *nwk* mutant phenotype.** (A) Schematic of *snx16* loss-of-function mutants. (B) Quantitative RT-PCR of *Snx16* and *CG10934* transcript levels. $n = 6$ for each sample. (C) Quantification of the mean satellite bouton number for muscle 4 NMJs. (D) Quantification of the mean bouton number for muscle 6/7 NMJs. (E) Elevated BMP signaling in *nwk* NMJs is suppressed in *Snx16;nwk* NMJs. Error bars are means ± SEM, and the number of samples averaged in each measurement is indicated at the base of each bar. *, $P < 0.05$; **, $P < 0.01$; ***, $P < 0.005$. Def, deficiency. Bars, 5 µm.

To examine the genetic relationship between *nwk* and *Snx16*, we generated double mutants of the null allele nwk^2 (Coyle et al., 2004) with *Snx16* mutants and found that allelic combinations of $Snx16^{PB}$, $Snx16^{\Delta1}$, and $Snx16^{\Delta2}$ significantly suppressed synaptic overgrowth in nwk^2 mutant larvae compared with genetically matched controls (Fig. 6, C and D). The *nwk* mutant synaptic overgrowth phenotype was restored in *Snx16*;*nwk* double mutants by reexpression of wild-type *Snx16* in neurons (Fig. 6 C), though we note that this rescue construct also produces mild synaptic overgrowth phenotypes in a wild-type background (Fig. 5 A). Collectively, our results show that multiple different loss-of-function alleles of *Snx16* suppress the *nwk* mutant phenotype. We also tested whether up-regulated BMP signaling in nwk^2 (O'Connor Giles et al., 2008) was suppressed by *Snx16* and found that both phosphorylated Mad (mothers against decapentaplegic, the downstream target of BMP receptors) and Trio protein levels at the NMJ were increased in *nwk* and suppressed in $Snx16^{PB}$;nwk^2 (Fig. 6 E). These results rule out the model that Snx16 acts as an upstream activator of Nwk, as in that case, *Snx16* mutants would be expected to phenocopy the *nwk* mutant, and instead indicate that synaptic overgrowth in *nwk* mutants results from a failure to down-regulate the growth-promoting activity of *Snx16*.

Snx16 is required for synaptic growth mediated by the BMP and Wg signaling cascades

Synaptic growth at the *Drosophila* larval NMJ requires the coordinated activities of several signal transduction cascades (Marqués and Zhang, 2006). One such pathway has been

Published April 4, 2011

demonstrated to function downstream of Nwk (O'Connor-Giles et al., 2008) and acts downstream of a retrograde signal mediated by the BMP family member Glass Bottom Boat and its receptors Tkv, Wit (Wishful Thinking), and Saxophone (Marqués and Zhang, 2006). Another prominent pathway is the presynaptic component of a cascade mediated by Wg and its receptors dFz2 (Frizzled 2) and Arrow (Franco et al., 2004; Miech et al., 2008). We tested whether Snx16 functions to promote signaling in these two pathways by generating double mutants between *Snx16* and BMP and Wg pathway mutants.

Dad (daughters against decapentaplegic) is a negative regulator of BMP signaling, and loss-of-function mutations in *dad* cause excessive BMP signaling and synaptic overgrowth (Sweeney and Davis, 2002; O'Connor-Giles et al., 2008). Loss of *Snx16* strongly suppressed synaptic overgrowth in *dad* mutants (Fig. 7 A). In addition, the synaptic overgrowth phenotypes caused by overexpression of Snx16-GFP and $Snx16^{3A}$-GFP were both suppressed by loss-of-function mutations in *wit*, the BMP receptor. These results suggest that, like *nwk*, synaptic growth mediated by *Snx16* requires BMP signaling. To test the involvement of the Wg pathway, we used *sgg* (*shaggy*)/glycogen synthase kinase-3β, which is negatively regulated by Wg. A dominant-negative *Sgg* mutant (sgg^{DN}) expressed in neurons mimics the presynaptic component of activated Wg signaling and causes synaptic overgrowth (Franco et al., 2004). Mutation of *Snx16* suppressed synaptic overgrowth caused by sgg^{DN} (Fig. 7 B). Nwk has not previously been implicated in Wg signaling, so we tested whether the synaptic overgrowth phenotype in *nwk* requires the activity of the Wg pathway, Loss-of-function mutations in *arrow*, the Wg coreceptor, cause only subtle synaptic growth defects (Fig. 7 B; Miech et al., 2008) but strongly suppress synaptic overgrowth in *nwk*, similar to results with *nwk* and BMP pathway mutants that have previously implicated Nwk in BMP signaling (O'Connor-Giles et al., 2008; Rodal et al., 2008). These results suggest that BMP- and Wg-mediated synaptic growth requires *Snx16* and that Nwk–SNX16-mediated membrane traffic is broadly used to constrain a variety of synaptic growth signals.

Overexpression of an activated version of the BMP receptor Tkv^{Q199D}, which signals in the absence of a ligand and coreceptor (Wieser et al., 1995; Hoodless et al., 1996), enhances the synaptic overgrowth phenotype of *nwk* mutants (O'Connor-Giles et al., 2008). We tested whether this mutant receptor might elucidate the fate of signaling receptors in the absence of Nwk–SNX16 interactions by cooverexpressing it in the *Snx16*-GFP– and $Snx16^{3A}$-GFP–overexpressing backgrounds. Strikingly, we found that tkv^{Q199D} dramatically enhanced the synaptic overgrowth phenotype of $Snx16^{3A}$-GFP but had no effect on *Snx16*-GFP (Fig. 7 C), suggesting that activated receptors were acutely sensitive to Nwk–SNX16-mediated traffic. Previously, we and others have not been able to detect rerouting of endogenous or overexpressed wild-type–signaling receptors at steady state in *nwk* mutant NMJs (O'Connor-Giles et al., 2008; Rodal et al., 2008). We reasoned that the activated receptor, which is sensitive to this genetic background, might reveal a subpopulation of the redistributed receptor. Indeed, we found that Tkv^{Q199D} (but not endogenous Tkv) was primarily found at the plasma membrane at steady state in *Snx16*-GFP–expressing NMJs but accumulated in intracellular structures, including Snx16-positive endosomes in $Snx16^{3A}$-GFP–expressing NMJs (Fig. 7 D), suggesting that Tkv^{Q199D} is specifically rerouted in this mutant, resulting in increased signaling.

Hrs down-regulates receptor signaling in the absence of SNX16

Although a dominant active Nwk-binding mutant of SNX16 promotes synaptic growth, loss-of-function *Snx16* mutants suppress synaptic growth, suggesting that SNX16 has a growth-promoting activity at the early endosome separate from its negative regulatory Nwk-binding activity. We hypothesized that because SNX16 is a peripheral membrane protein on endosomes, it may act by limiting the internalization of activated receptors into MVBs via the ESCRT pathway (Raiborg and Stenmark, 2009). In this model (Fig. 8 A), attenuation of receptor signaling is balanced between SNX16–Nwk-mediated sorting to the recycling endosome and ESCRT-mediated internalization of the receptor into the endosomal lumen, with SNX16 representing a branch point between these two pathways. We predicted that if MVB formation were inhibited, *Snx16* loss-of-function mutants would produce synaptic overgrowth, the opposite phenotype from that of *Snx16*;*nwk*, *Snx16*;*dad*, or *Snx16*;sgg^{DN} double mutants. To test this hypothesis, we made double mutants between *Snx16* and hrs^{D28}, a mutant in a component of the ESCRT machinery (Lloyd et al., 2002). Hrs is broadly used in many cell types for endosomal cargo traffic, and both *hrs* single and *hrs*;*Snx16* double mutants are sick and die between early larval and early pupal stages. We examined NMJ growth in single and double mutants. *hrs* mutants have been shown to have no defect in synaptic growth (Lloyd et al., 2002); however, *hrs;Snx16* double mutants exhibited significant overproliferation of overall bouton number and satellite bouton number compared with *hrs* single mutants (Fig. 8 B), which is in sharp contrast to the reduction in synaptic growth in the *Snx16* mutant backgrounds (Figs. 6 and 7). These results suggest that receptor signaling in *Snx16* animals is attenuated by internalization into the endosomal lumen, whereas animals containing wild-type *Snx16* do not depend on MVB function to attenuate signaling, presumably because of SNX16–Nwk-mediated sorting to the recycling endosome.

To further explore the relationship between MVB formation and Snx16 function, we used electron microscopy to examine the ultrastructure of synaptic boutons in *Snx16*-GFP– and $Snx16^{3A}$-GFP–overexpressing larvae, in which synaptic overgrowth is apparent (Fig. 5). Morphologically distinct MVBs are rarely observed in thin sections of wild-type synaptic boutons by electron microscopy but were frequently observed in $Snx16^{3A}$-GFP–overexpressing boutons (Fig. 8 C). We hypothesize that this increase in MVB formation results from stalled membrane traffic at the early endosome when SNX16–Nwk-mediated traffic is disrupted. Collectively, these results support a model in which SNX16 functions at the intersection of a branch point in the endosomal traffic of synaptic growth receptors from the early endosome to either the recycling endosome or to a degradative MVB pathway.

Published April 4, 2011

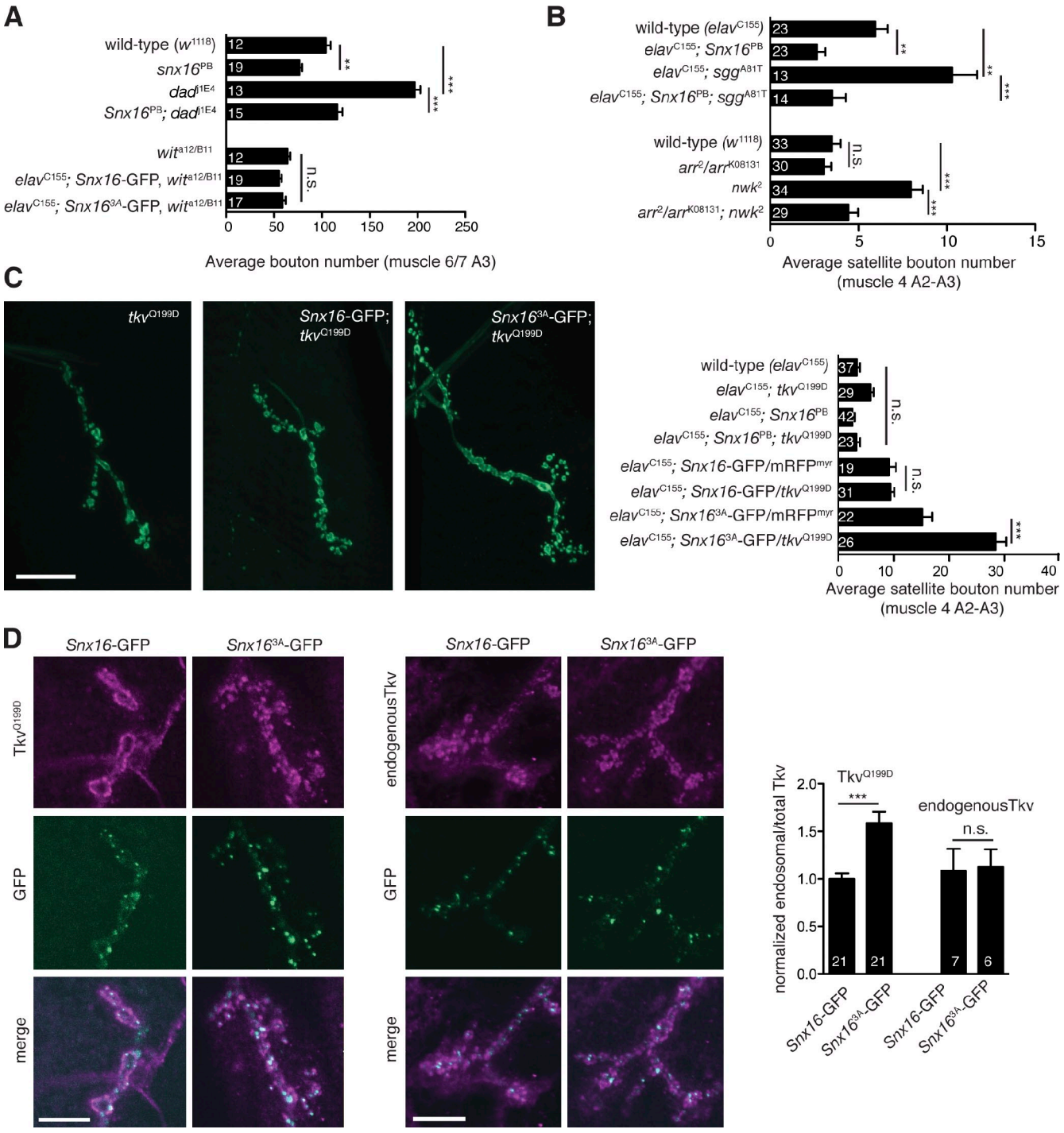

Figure 7. ***Snx16* is required for synaptic growth mediated by BMP and Wg cascades.** (A) Quantification of the mean bouton number for muscle 6/7 NMJs from larvae defective in BMP signaling. (B) Quantification of the mean satellite bouton number for muscle 4 NMJs defective in Wg signaling. (C) Representative confocal images of muscle 4 NMJs from *Snx16-GFP;tkv*^{Q199D} larvae and quantification of the mean satellite bouton number. Control UAS data are identical to Fig. 5 E. (D) Localization of Tkv^{Q199D} and endogenous Tkv to Snx16-positive endosomes. Quantification shows muscle 4, segments A2–A4, α-Tkv–integrated density in GFP-positive pixels relative to total NMJ α-Tkv–integrated density in single confocal sections. Error bars are means ± SEM, and the number of samples averaged in each measurement is indicated at the base of each bar. **, $P < 0.01$; ***, $P < 0.005$. Bars: (C) 20 µm; (D) 10 µm.

Discussion

Endocytic membrane traffic regulates signaling by synaptic growth factor receptors and may be used as a point of control in tuning receptor traffic in response to neuronal activity. The neuronal F-BAR/SH3 protein Nwk is involved in endocytic membrane traffic that attenuates synaptic growth signaling, but the mechanism by which it acts has been unknown. Here, we identify a physical interaction between Nwk and the early endosomal protein SNX16 that is critical for down-regulating the synaptic growth-promoting activity of SNX16. This interaction may bring together the actin-polymerizing activity of the first SH3 domain

Published April 4, 2011

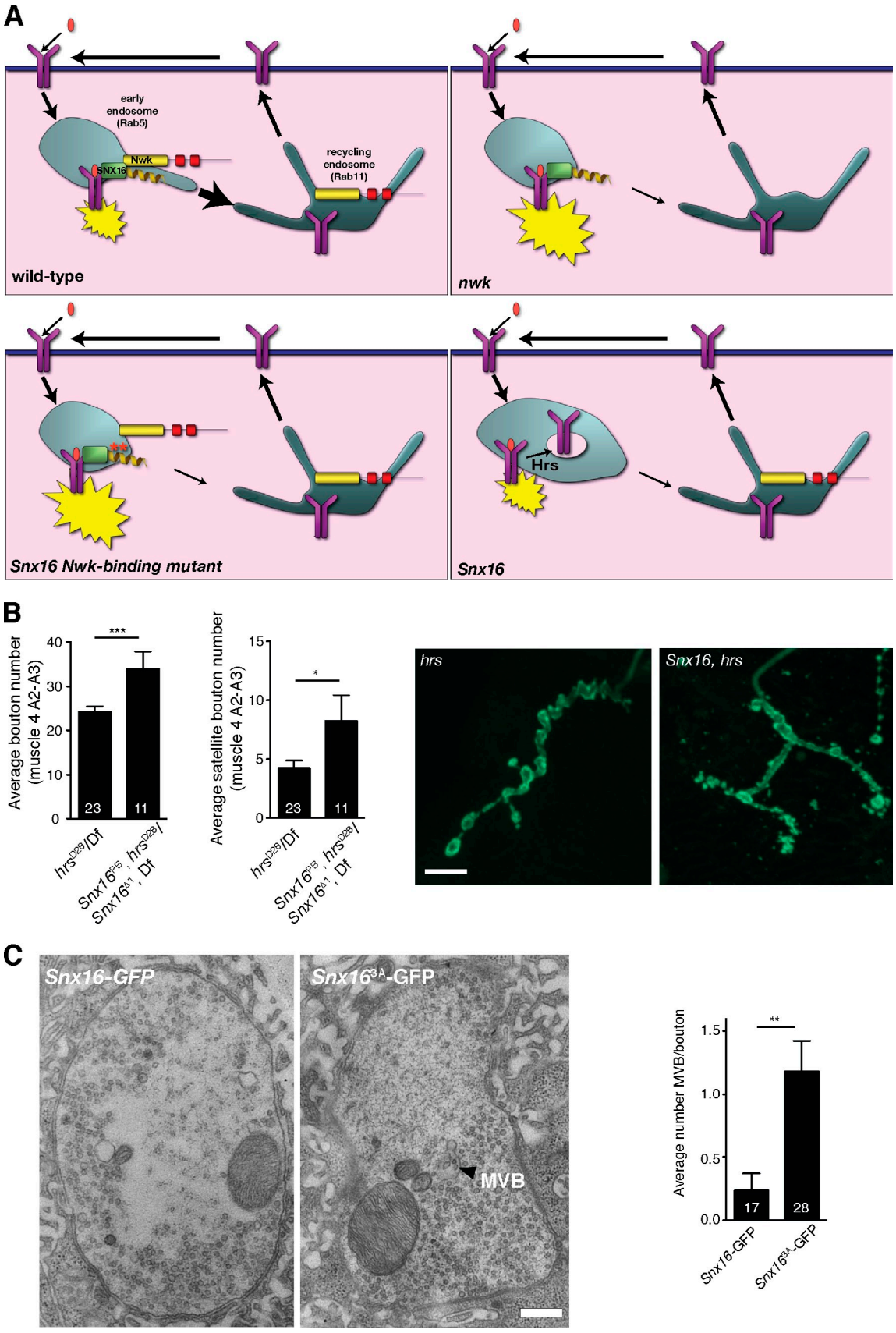

Figure 8. **A branched pathway model for the attenuation of synaptic growth signals by endosomal traffic.** (A) Model depicting how Nwk and SNX16 may drive tubulation-based sorting of synaptic growth receptors from the signal-permissive early endosome to the recycling endosome, where signaling (indicated by yellow starbursts) is attenuated. In the absence of Nwk or Nwk–SNX16 interactions, receptors are retained in the early endosome. In the

Published April 4, 2011

of Nwk (Rodal et al., 2008) with the potential lipid-binding/tubulating activities of the F-BAR domain of Nwk and the PX domain of SNX16, driving tubule-based membrane flux from early to recycling endosomes.

Function of the interaction between Nwk and SNX16

Sorting nexins form a large family of proteins that share a common phosphoinositide-binding PX domain and are involved in diverse aspects of membrane traffic (Cullen, 2008). The best-characterized members of this family are the sorting nexin–BAR family, including Snx1 (tied to endosome-to-Golgi traffic) and Snx9 (tied to the internalization step of endocytosis), which each contains both a lipid-tubulating BAR domain and a PX domain. Crystal structures and functional studies of Snx9 have shown that its BAR and PX domains form a single lipid-binding and -deforming module with combined specificities that neither domain exhibits alone (Pylypenko et al., 2007; Yarar et al., 2008; Wang et al., 2008a). As such, SNX16–Nwk interactions may form an analogous F-BAR/PX module via an intermolecular rather than intramolecular interaction. We have not been able to purify sufficient amounts of SNX16 to directly test its effects on lipid binding by Nwk; therefore, further analysis of their interaction will require an approach to isolate SNX16 in vitro. Interestingly, the SNX16–Nwk interaction depends on a region of Nwk surrounding its second SH3 domain, raising the possibility that this region of Nwk may exert intramolecular effects on the amino-terminal F-BAR domain, as has previously been shown for other F-BAR proteins (Rao et al., 2010). Furthermore, Nwk binds to the coiled-coil region of SNX16 (Fig. 1), which is involved in SNX16 dimerization (Hanson and Hong, 2003; Choi et al., 2004), suggesting that Nwk may act on SNX16 by affecting its dimerization state.

Mammalian SNX16 has been implicated in the trafficking of the EGF receptor from early to late endosomes, which may mediate down-regulation of receptor signaling (Hanson and Hong, 2003; Choi et al., 2004). However, the mechanism by which SNX16 promotes this trafficking step is not understood and no loss-of-function studies on SNX16 have been reported. A mutant of mammalian SNX16 that lacks 60 aa corresponding to the *Drosophila* SNX16 Nwk-binding site (Fig. 1 B) blocks trafficking of SNX16 and EGF to late endosomes, leading to increased EGF signaling (Hanson and Hong, 2003). Interestingly, the F-BAR protein FBP17 has been reported to interact with SNX2 (Fuchs et al., 2001). These results raise the possibility that BAR family–sorting nexin interactions may be broadly used to control membrane traffic in cells.

Synaptic growth signaling is attenuated by transient interactions between SNX16 and Nwk compartments

We found that *Drosophila* SNX16 localizes to an early endosomal compartment at the NMJ defined by the small GTPases Rab4 and Rab5 (Figs. 2 and 3). This compartment accumulates signaling receptors, such as the BMP receptors Tkv and Wit (Fig. 3; Wang et al., 2007), and signaling is amplified when receptors are stalled in this compartment (Wang et al., 2007), suggesting that the SNX16 compartment is an active site of signaling. By identifying specific *Snx16* mutants that disrupt interactions with Nwk, we were able to separate the requirements for receptor down-regulation at early endosomes and show that activated receptors specifically require SNX16–Nwk-mediated traffic to recycle to the plasma membrane (Fig. 7).

We previously observed that Nwk colocalizes with the recycling endosome marker Rab11 in fixed tissue and cooperates with Cdc42, which is thought to function at the recycling endosome, to activate WASp/Arp2/3-mediated actin polymerization (Rodal et al., 2008). Together with the result that *rab11* mutants exhibit synaptic overgrowth similar to *nwk* mutants (Khodosh et al., 2006), we concluded that Nwk functions at recycling endosomes, which are downstream of early endosomes. Here, we show that Nwk tagged with fluorescent proteins localizes to novel punctate structures in heterologous cells (Fig. 2) and nerve terminals (Fig. 4). These puncta had not been observed using anti-Nwk antibodies against either endogenous or overexpressed Nwk in fixed tissue (Rodal et al., 2008), as they are poorly preserved upon fixation (Fig. 4). In living synapses, Rab11 colocalizes with Nwk to mobile puncta, SNX16-containing early endosomes interact transiently with Nwk puncta, and inhibition of the GTPase dynamin blocks separation of these compartments (Fig. 4). Dynamin inhibition has previously been shown to disrupt endosomal function in the fly NMJ (Wucherpfennig et al., 2003), so we cannot be certain that the collapse of SNX16–Nwk compartments under these conditions is caused by the specific interactions of these proteins with dynamin. However, because SNX16–Nwk interactions lead to the down-regulation of synaptic growth signals, our data are consistent with a model in which the exchange of receptors from the SNX16 endosome to the Nwk/Rab11 endosome leads to the attenuation of receptor signaling. Binding of Nwk to the cytoplasmic tail of the BMP receptor Tkv may mediate this event (O'Connor-Giles et al., 2008), but further experiments will be required to directly examine cargo transfer in the future. Because there are significant cytoplasmic pools of both Nwk and SNX16, we also cannot exclude the contribution of these soluble proteins to membrane traffic in the nerve terminal or the possibility that overexpression of Nwk and Snx16 to visualize live trafficking events does not faithfully recapitulate the behaviors of endogenous proteins. However, the transient interaction of Nwk and SNX16 puncta correlates well with our genetic results showing that *nwk* attenuates a synaptic growth-promoting activity of *Snx16* at early endosomes.

Because Nwk- and SNX16-labeled compartments transiently interact in nerve terminals, temporal control of the interaction

absence of SNX16, receptors are down-regulated by internalization into the endosomal lumen. (B) Representative confocal images of Cpx-stained NMJs from $hrs^{D28}/Df(exel6277)$ and $Snx16^{PB}$, $hrs^{D28}/Snx16^{A1}$, $Df(exel6277)$ larvae and quantification of the mean bouton number. (C) Overexpression of $SNX16^{3A}$ increases MVB number. Electron micrographs of type 1b boutons from SNX16-GFP and $SNX16^{3A}$-GFP–expressing larvae and quantification of MVB structures. Error bars are means ± SEM, and the number of samples averaged in each measurement is indicated at the base of each bar. *, $P < 0.05$; **, $P < 0.01$; ***, $P < 0.005$. Bars: (B) 10 µm; (C) 200 nm.

Published April 4, 2011

between their lipid-binding domains may provide a mechanism to acutely drive membrane tubulation in a regulated fashion. Furthermore, the association of SNX16 with endosomes depends on phosphoinositides, as the phosphatidylinositol 3-kinase inhibitor wortmannin disrupts localization of SNX16 in cultured cells (Fig. 2), indicating that regulation of phospholipid composition may also contribute to the membrane-deforming activities of SNX16 and Nwk.

Snx16 acts at a branch point between endosomal sorting pathways

We found that *Snx16* loss-of-function mutants suppress synaptic overgrowth resulting from loss of Nwk-mediated traffic as well as from activation of Wg and BMP signaling pathways (Figs. 6 and 7). These data suggest that SNX16 plays an active role in promoting synaptic growth at the endosome, aside from its function in signal attenuation through Nwk. We found that Snx16 is required to restrict synaptic growth when MVB formation is hampered in *hrs* mutants (Fig. 8), suggesting that receptor entry into the endosomal lumen is an alternative signal attenuation pathway. Furthermore, we found that overexpression of a mutant *Snx16* that cannot bind Nwk promotes the accumulation of endosomal structures at the NMJ (Figs. 7 D and 8 C) and drives excess synaptic growth, suggesting that Snx16 may play a role in MVB maturation and acts at the branch point between endosomal sorting pathways. Defining the mechanism by which SNX16 promotes synaptic growth will require further structure–function analysis of the active domains of the protein aside from its Nwk-binding coiled coil.

Activity dependence of synaptic receptor endocytosis

Traffic through endocytic compartments has proven to be a critical point of regulation in the nervous system. Synaptic vesicle endocytosis is controlled by synaptic activity through calcium-dependent dephosphorylation of endocytic proteins (Cousin, 2009), and postsynaptic trafficking of AMPA receptors through the recycling endosome is increased in response to activity via the calcium-dependent motor myosin V (Wang et al., 2008b). Rab5-positive compartments at the *Drosophila* NMJ have been previously characterized for their role in the synaptic vesicle cycle (Wucherpfennig et al., 2003), and it will be interesting to determine how receptor-mediated endocytosis and synaptic vesicle endocytosis are coordinately or separately regulated in response to activity. Synaptic growth at the *Drosophila* NMJ is positively regulated by calcium influx through voltage-gated calcium channels (Rieckhof et al., 2003), and endosome number increases in response to activity (Akbergenova and Bykhovskaia, 2009). It is tempting to speculate that calcium influx acts through conserved mechanisms for modulating membrane dynamics to delay the attenuation of receptor signaling by SNX16–Nwk-mediated traffic, leading to increased synapse growth in response to activity. A key future goal will be to determine specific points of activity-dependent regulation of membrane traffic in presynaptic endosomes.

Materials and methods

Fly stocks and generation of *Snx16* mutants

Flies were cultured using standard media and techniques. UAS-*Snx16* and UAS-*Snx16*-GFP lines were constructed in pUAST (Brand and Perrimon, 1993) carrying the *Snx16* cDNA (clone SD19533; Berkeley *Drosophila* Genome Project), and point mutations were generated by site-directed mutagenesis. Sequence-verified constructs were injected into w^{1118} flies at the Duke Model Systems Transgenic Facility or at Genetic Services, Inc. The *P* element line P(EPgy2)EY10175, carrying an insertion 39 bp 5′ to the Snx16 start codon, was isogenized and crossed to *w;P/CyOΔ2-3* to mobilize the insertion. Approximately 500 candidate white-eyed lines were tested by PCR across the *P* element insertion site, and *Snx16Δ* lines and a precise excision ($Snx16^{\Delta pre}$) were verified by sequencing across the deletion. Nwk-mRFP and Tkv^{Q199D} lines were obtained from K. O'Connor-Giles (University of Wisconsin, Madison, WI), and Tkv-GFP flies were obtained from M. González-Gaitán (University of Geneva, Geneva, Switzerland). All other fly strains were obtained from the Bloomington *Drosophila* Stock Center or the Exelixis Collection (Harvard Medical School).

RT-PCR

Quantitative RT-PCR was performed using a real-time PCR system (7300 Real-Time PCR System; Applied Biosystems). Total RNA was extracted from 10–15 adult flies per sample, single-stranded cDNA was synthesized, and PCR was performed in triplicate for each of two independent total RNA samples per genotype using an SYBR green PCR master mix (QuantiTect; QIAGEN). A final dissociation step was performed to evaluate product integrity, and reaction samples were run on a 1.2% agarose gel and stained with ethidium bromide. The primer sequences were as follows: *Act88F*, 5′-ACTTCTGCTGGAAGGTGGAC-3′ and 5′-ATCCGCAAGGATCTGTATGC-3′; *Snx16*, 5′-ACTGCGCGAGGAGATGAACGA-3′ and 5′-CTCCGATTGGCGAAGGTCTACT-3′; and *CG10934*, 5′-TGAAAGAGCAGAGCCAACACG-3′ and 5′-CGACACAACGCTCTTCTTCTTCTC-3′.

Antibodies

A fragment of *Snx16* encoding aa 230–408 was cloned into pGEX-4T (Promega), expressed in BL21(DE3) *E. coli*, and purified from sarkosyl-solubilized extracts using glutathione agarose followed by resolubilization in Triton X-100 (Frangioni and Neel, 1993). The purified fusion protein was dialyzed into PBS and injected into guinea pigs (Invitrogen). Guinea pig sera were then affinity purified against a His-tagged fragment of SNX16 encoding aa 335–407, purified as previously described for the His-tagged WASp WH1 domain using the antigen immobilized on nitrocellulose (Rodal et al., 2008), and used at 1:250 for immunohistochemistry (IHC) and at 1:1,000 for immunoblots (IBs). α-Tkv antibodies (1:200 for IHC) were provided by M.B. O'Connor (University of Minnesota, Minneapolis, MN). α-Nwk (antibody 970; 1:1,000 for IHC and 1:2,000 for IBs; Coyle et al., 2004), α-Dap160 (1:20,000 for IBs; provided by G. Davis, University of California, San Francisco, San Francisco, CA; Roos and Kelly, 1998), polyclonal α-mRFP (1:250 for IHC; Takara Bio Inc.), α-GFP (1:1,000 for IBs; Abcam), α-Hrs (1:1,000 for IHC; provided by H. Bellen, Baylor College of Medicine, Houston, TX; Lloyd et al., 2002), α-phospho–Mad PS1 (1:1,000 for IHC; provided by P. Ten Dijk, Leiden University, Leiden, Netherlands; Persson et al., 1998), α-Trio (1:10 for mAb supernatant IHC; Awasaki et al., 2000), and α-Rab11 (1:100 for IHC; BD; Khodosh et al., 2006) antibodies have been described previously. All mAb's were provided by the Developmental Studies Hybridoma Bank (University of Iowa). Secondary antibodies for imaging were conjugated to Cy2 or Rhodamine Red-X (Jackson ImmunoResearch Laboratories, Inc.).

Yeast two-hybrid and GST pull-down assays

Yeast two-hybrid assays were conducted using the Matchmaker system (Takara Bio Inc.). Full-length Nwk was cloned into pAS2-1, transformed into yeast strain AH109, and used to screen 1.5×10^6 transformants of a pACT2 Matchmaker library generated from whole *Drosophila* adult cDNA (Takara Bio Inc.) for growth on minimal media lacking leucine, tryptophan, histidine, and adenine. Candidate colonies were further selected for growth on the aforementioned media containing 10 mM 3-aminotriazole. DNA from colonies passing this secondary screen was purified and retransformed into AH109 yeast cells carrying plasmid pGBKT7-NWK. Directed two-hybrid tests were conducted with NWK constructs in pGBKT7 (Rodal et al., 2008) and *Snx16* constructs in pACT2 (Takara Bio Inc.). The Nwk SH3a point mutant W581A and the SH3b point mutant W677A were previously described (Rodal et al., 2008). Yeast cells containing both prey and bait constructs were selected on minimal media lacking leucine

Published April 4, 2011

and tryptophan and then restruck on plates lacking histidine and containing 3-aminotriazole. Yeast colonies were scored for growth after 3 d at 30°C.

GST pull-down assays were conducted as previously described (Rodal et al., 2008). In brief, GST fusions were purified from bacterial lysates in PBS with 0.5 mM dithiothreitol and used to precipitate binding partners from wild-type and elav-Gal4^{C155};UAS-*Snx16*-GFP or UAS-*Snx16* fly head extracts made in 25 mM Tris, pH 7.5, 75 mM NaCl, and 0.2% Nonidet P-40 (Fig. 1, C and D) or from BL21 DE3 Rosetta cells (Invitrogen) coexpressing GST-Nwk and pET28a, pET28a-*Snx16* (aa 220–407), or pET28a-*Snx16*^{3A} (aa 220–407) and bound to glutathione agarose in 25 mM Tris, pH 7.5, and 75 mM KCl (Fig. 1 E).

Cell culture

rab5, *rab11*, *Snx16*, and *nwk* cDNAs were tagged with mRFP, mCherry, and GFP under the control of the actin promoter or UAS sequences using Gateway technology (Invitrogen). Kc167 or S2 cells (Cherbas and Cherbas, 1998) were cultured according to standard protocols and transfected using Effectene reagent (QIAGEN). Transfected cells were incubated for 2–3 d at 20°C and then fixed for 15 min in PBS containing 4% formaldehyde. Cells were washed twice with PBS and imaged for mCherry or mRFP and GFP localization on a microscope (Axioplan; Carl Zeiss; see the following section). For Fig. 2 (B, C, and E), cells were spread for 1 h on coverslips coated with concanavalin A before fixation (Rogers et al., 2003). For wortmannin experiments, cells were transfected as in this paragraph, washed with PBS, and treated with 100 µM wortmannin or DMSO alone as a control for 45 min before fixation and imaging. For transferrin uptake assays, Kc167 cells transfected as in this paragraph with pUASt–human transferrin receptor (Strigini and Cohen, 2000), actin promoter–Gal4, and the indicated constructs were incubated at room temperature with culture media containing 5 µg/ml Alexa Fluor 546–labeled transferrin (Invitrogen). Cells were washed twice with PBS and then fixed and processed as in this paragraph.

IHC and analysis of NMJ morphology

For analysis of NMJ morphology and protein localization at the NMJ, flies were cultured at low density at 25°C. Wild-type controls for each experiment were selected to be closely genetically matched to experimental genotypes. For *hrs* and *hrs;Snx16* mutants, which survived poorly, first and second instar larvae were transferred to grape juice plates and grown to third instar. Wild-type and *Snx16* animals grew large and pupated much more quickly than *hrs* mutants under these conditions and, thus, were not included as controls. Wandering third instar larvae were dissected in calcium-free HL3.1 saline (Feng et al., 2004) and fixed for 30 min in HL3.1 containing 4% formaldehyde before antibody staining.

Larvae were mounted in 70% glycerol in PBS and imaged at room temperature on a microscope (Axioplan) equipped with a laser-scanning head (LSM510; Carl Zeiss) and oil immersion 40× 1.3 NA or 100× 1.3 NA objectives. Images were acquired with Pascal software. For analysis of NMJ morphology, NMJs on muscle 6/7, segment A3, and muscle 4, segments A2–A3, were selected for analysis. NMJs were stained with α-complexin (Cpx)– and Cy2-conjugated secondary antibodies (Huntwork and Littleton, 2007) and α-Discs Large– and Rhodamine Red-X–conjugated secondary antibodies (Parnas et al., 2001). Both type 1b and type 1s boutons were quantified on muscle 6/7. Only type 1b innervation, delineated by extensive postsynaptic anti–Discs Large staining, was quantified on muscle 4. Satellite boutons were defined as strings of five or fewer boutons extending from the main axis of the NMJ.

For dynasore experiments, dissected larvae were incubated for 10 min in HL3.1 with 90 mM KCl, 2 mM $CaCl_2$ (Verstreken et al., 2008), and 100 µm dynasore (Sigma-Aldrich) in 0.2% DMSO or 0.2% DMSO alone. High-potassium solution was used to ensure that all synaptic dynamin was cycled through a blockable state by stimulating complete synaptic vesicle release and reuptake (Ramaswami et al., 1994). Animals were briefly washed in HL3.1 and then fixed for 30 min in HL3.1 with 4% formaldehyde (note that fixation without detergent extraction preserves Nwk puncta) before imaging by laser-scanning confocal microscopy (which allows rigorous emission discrimination compared with spinning-disk confocal microscopy for colocalization analyses without cross talk between channels).

Live imaging

Wandering third instar larvae expressing *Snx16*-GFP and *nwk*-mRFP under the control of the panneuronal GAL4 driver *elav*^{C155} were dissected as in the previous section, mounted in HL3.1 under a coverslip, and imaged at room temperature with a 63× 1.4 NA objective on a microscope (Observer Z1; Carl Zeiss) equipped with a spinning-disk confocal head (CSU-X1; Yokagawa) and an electron microscope charge-coupled device camera (QuantEM 512SC; 3i People, Inc.). Confocal stacks of NMJs were collected at a frame rate of ∼1 stack/2.5 s. Videos were created from maximum intensity projections of these stacks using SlideBook software (3i People, Inc.) and displayed at 10× live speed.

Electron microscopy

Wandering third instar larvae expressing *Snx16*-GFP or *Snx16*^{3A}-GFP were dissected, fixed, and processed for electron microscopy as previously described (Akbergenova and Bykhovskaia, 2009). In brief, filleted larvae were fixed in 1% glutaraldehyde, 4% formaldehyde, and 0.1 M sodium cacodylate for 2 h at room temperature and then 4°C overnight. After washing in 0.1 M sodium cacodylate and 0.1 M sucrose, samples were postfixed for 1 h in 1% osmium tetroxide, dehydrated through a graded series of ethanol and acetone, and embedded in epoxy resin (Embed 812; Electron Microscopy Sciences). Thin sections (70–90 nm) were collected on Formvar/carbon-coated copper slot grids and contrasted with lead citrate. For immunoelectron microscopy, samples were fixed for 20 min in 4% paraformaldehyde in PBS and blocked for 1 h in 1% BSA in PBS followed by incubation for 3 h in α-GFP (ab6556; Abcam) and then 2 h in a doubly conjugated Alexa Fluor 594 and 1.4-nm nanogold secondary antibody (Nanoprobes). The gold signal was enhanced for 7 min using Gold Enhance (Nanoprobes) followed by a second 1 h fixation in 1% glutaraldehyde and 4% paraformaldehyde and then embedded and sectioned as for unlabeled samples. Thin sections (70–90 nm for Fig. 8 C and 50–70 nm for Fig. 3 F) were imaged at a 49,000× magnification at 80 kV on an electron microscope (Tecnai G2 Spirit; FEI) equipped with an charge-coupled device camera (Advanced Microscopy Techniques). Type 1b boutons with small clear vesicles (Atwood et al., 1993; Jia et al., 1993) were scored for the presence of MVBs.

Electrophysiology

Evoked postsynaptic currents were recorded from muscle 6 of segment A3 in third instar larvae using two-electrode voltage clamp (OC-725; Warner Instruments) at a –80-mV holding potential (Acharya et al., 2006; Barber et al., 2009). All experiments were performed in a modified HL3.1 solution (70 mM NaCl, 5 mM KCl, 4 mM $MgCl_2$, 2 mM $CaCl_2$, 10 mM $NaHCO_3$, 115 mM sucrose, and 5 mM Hepes, pH 7.2). Animals were pretreated with 100 µm dynasore or DMSO control for 3–5 min before beginning stimulation and recording, and dynasore or DMSO were present throughout the recording. Data acquisition and analysis were performed using pClamp software (Axon Instruments). For stimulation, nerves were cut close to the ventral ganglion and sucked into a pipette filled with working solution. The nerve was stimulated at 20 Hz using a programmable pulse stimulator (Master-8; A.M.P.I.).

Image and statistical analyses

All image analysis was performed in ImageJ (National Institutes of Health), and quantitative colocalization was performed using the JACoP (Just Another Colocalization Plugin) plugin (Bolte and Cordelières, 2006). For quantification of Trio protein levels from 2D projections of confocal stacks, mean Trio and Cpx levels were measured within Cpx-positive NMJs on muscle 6/7, segments A2–A4. The muscle background mean intensity for both signals was also measured and subtracted from the NMJ measurement. Mean background-subtracted Trio intensity was then normalized to background-subtracted mean Cpx intensity. Mean Cpx intensity did not vary between genotypes. Phospho-Mad intensities were measured within α-Csp (cysteine-string protein; Zinsmaier et al., 1994)–positive NMJs. For quantification of Tkv localization, SNX16-GFP pixels were selected from single confocal sections of muscle 6/7, segments A2–A4, and the integrated density of Tkv in these structures was measured relative to the entire NMJ Tkv signal in the section. *Snx16*^{3A} data were separately normalized to the *Snx16* mean for either Tkv^{Q199D} or endogenous Tkv because of their different expression levels above the background.

All errors shown are means ± SEM, and the number of samples averaged in each measurement in the bar graphs is indicated at the base of each bar. The statistical significance was calculated using Prism software (GraphPad Software) using analysis of variance followed by pairwise Tukey's tests or using Student's *t* tests in which only two groups were compared, with an asterisks denoting p-value: *, $P < 0.05$; **, $P < 0.01$; and ***, $P < 0.005$.

Online supplemental material

Fig. S1 (associated with Fig. 1) shows alignment of SNX16 homologues. Fig. S2 (associated with Fig. 3) shows specificity of α-SNX16 antibodies.

Fig. S3 (associated with Fig. 4) shows electrophysiological analysis of larval NMJs treated with dynasore. Videos 1–3 (associated with Fig. 4) show the transient association of Nwk-mRFP and SNX16-GFP in synaptic boutons. Online supplemental material is available at http://www.jcb.org/cgi/content/full/jcb.201009052/DC1.

We thank the Developmental Studies Hybridoma Bank, the Exelixis Collection at Harvard Medical School, the *Drosophila* Genome Resource Center, The Bloomington *Drosophila* Stock Center, Kate O'Connor-Giles, Michael O'Connor, Marcos González-Gaitán, Hugo Bellen, and Michael Marr for reagents; Daniela Nicastro, Bruce Goode, and Piali Sengupta for equipment; Defne Yarar, Katharine Sepp, Joost Schulte, Bruce Goode, Robin Stevens, and Sarah Huntwork-Rodriguez for helpful scientific discussions; and Anne Yu, Danielle Pigneri, Betty Yang, Stephanie Shim, Rebecca Rodal, and Rebecca Motola-Barnes for technical assistance.

A.A. Rodal was supported by postdoctoral grants from the Damon Runyon Cancer Research Foundation and the Charles King Trust of the Medical Foundation and a K99/R00 award from the National Institute of Neurological Disorders and Stroke (K99NS060947). J.T. Littleton was supported by a National Institutes of Health award (NS43244).

Submitted: 9 September 2010
Accepted: 9 March 2011

References

Acharya, U., M.B. Edwards, R.A. Jorquera, H. Silva, K. Nagashima, P. Labarca, and J.K. Acharya. 2006. *Drosophila melanogaster* Scramblases modulate synaptic transmission. *J. Cell Biol.* 173:69–82. doi:10.1083/jcb.200506159

Akbergenova, Y., and M. Bykhovskaia. 2009. Enhancement of the endosomal endocytic pathway increases quantal size. *Mol. Cell. Neurosci.* 40:199–206. doi:10.1016/j.mcn.2008.10.005

Atwood, H.L., C.K. Govind, and C.F. Wu. 1993. Differential ultrastructure of synaptic terminals on ventral longitudinal abdominal muscles in *Drosophila* larvae. *J. Neurobiol.* 24:1008–1024. doi:10.1002/neu.480240803

Awasaki, T., M. Saito, M. Sone, E. Suzuki, R. Sakai, K. Ito, and C. Hama. 2000. The *Drosophila* trio plays an essential role in patterning of axons by regulating their directional extension. *Neuron*. 26:119–131. doi:10.1016/S0896-6273(00)81143-5

Ball, R.W., M. Warren-Paquin, K. Tsurudome, E.H. Liao, F. Elazzouzi, C. Cavanagh, B.S. An, T.T. Wang, J.H. White, and A.P. Haghighi. 2010. Retrograde BMP signaling controls synaptic growth at the NMJ by regulating trio expression in motor neurons. *Neuron*. 66:536–549. doi:10.1016/j.neuron.2010.04.011

Barber, C.F., R.A. Jorquera, J.E. Melom, and J.T. Littleton. 2009. Postsynaptic regulation of synaptic plasticity by synaptotagmin 4 requires both C2 domains. *J. Cell Biol.* 187:295–310. doi:10.1083/jcb.200903098

Bolte, S., and F.P. Cordelières. 2006. A guided tour into subcellular colocalization analysis in light microscopy. *J. Microsc.* 224:213–232. doi:10.1111/j.1365-2818.2006.01706.x

Bonifacino, J.S., and R. Rojas. 2006. Retrograde transport from endosomes to the *trans*-Golgi network. *Nat. Rev. Mol. Cell Biol.* 7:568–579. doi:10.1038/nrm1985

Brand, A.H., and N. Perrimon. 1993. Targeted gene expression as a means of altering cell fates and generating dominant phenotypes. *Development*. 118:401–415.

Cherbas, L., and P. Cherbas. 1998. Cell culture. *In Drosophila*: A Practical Approach. D.B. Roberts, editor. IRL Press, Oxford, England, UK/New York. 319–346.

Choi, J.H., W.P. Hong, M.J. Kim, J.H. Kim, S.H. Ryu, and P.G. Suh. 2004. Sorting nexin 16 regulates EGF receptor trafficking by phosphatidylinositol-3-phosphate interaction with the Phox domain. *J. Cell Sci.* 117:4209–4218. doi:10.1242/jcs.01233

Cousin, M.A. 2009. Activity-dependent bulk synaptic vesicle endocytosis—a fast, high capacity membrane retrieval mechanism. *Mol. Neurobiol.* 39:185–189. doi:10.1007/s12035-009-8062-3

Coyle, I.P., Y.H. Koh, W.C. Lee, J. Slind, T. Fergestad, J.T. Littleton, and B. Ganetzky. 2004. Nervous wreck, an SH3 adaptor protein that interacts with Wsp, regulates synaptic growth in *Drosophila*. *Neuron*. 41:521–534. doi:10.1016/S0896-6273(04)00016-9

Cullen, P.J. 2008. Endosomal sorting and signalling: an emerging role for sorting nexins. *Nat. Rev. Mol. Cell Biol.* 9:574–582. doi:10.1038/nrm2427

Delgado, R., C. Maureira, C. Oliva, Y. Kidokoro, and P. Labarca. 2000. Size of vesicle pools, rates of mobilization, and recycling at neuromuscular synapses of a *Drosophila* mutant, *shibire*. *Neuron*. 28:941–953. doi:10.1016/S0896-6273(00)00165-3

Dickman, D.K., Z. Lu, I.A. Meinertzhagen, and T.L. Schwarz. 2006. Altered synaptic development and active zone spacing in endocytosis mutants. *Curr. Biol.* 16:591–598. doi:10.1016/j.cub.2006.02.058

Feng, Y., A. Ueda, and C.F. Wu. 2004. A modified minimal hemolymph-like solution, HL3.1, for physiological recordings at the neuromuscular junctions of normal and mutant *Drosophila* larvae. *J. Neurogenet.* 18:377–402. doi:10.1080/01677060490894522

Franco, B., L. Bogdanik, Y. Bobinnec, A. Debec, J. Bockaert, M.L. Parmentier, and Y. Grau. 2004. Shaggy, the homolog of glycogen synthase kinase 3, controls neuromuscular junction growth in *Drosophila*. *J. Neurosci.* 24:6573–6577. doi:10.1523/JNEUROSCI.1580-04.2004

Frangioni, J.V., and B.G. Neel. 1993. Solubilization and purification of enzymatically active glutathione S-transferase (pGEX) fusion proteins. *Anal. Biochem.* 210:179–187. doi:10.1006/abio.1993.1170

Frost, A., V.M. Unger, and P. De Camilli. 2009. The BAR domain superfamily: membrane-molding macromolecules. *Cell*. 137:191–196. doi:10.1016/j.cell.2009.04.010

Fuchs, U., G. Rehkamp, O.A. Haas, R. Slany, M. König, S. Bojesen, R.M. Bohle, C. Damm-Welk, W.D. Ludwig, J. Harbott, and A. Borkhardt. 2001. The human formin-binding protein 17 (FBP17) interacts with sorting nexin, SNX2, and is an MLL-fusion partner in acute myelogeneous leukemia. *Proc. Natl. Acad. Sci. USA*. 98:8756–8761. doi:10.1073/pnas.121433898

Hanson, B.J., and W. Hong. 2003. Evidence for a role of SNX16 in regulating traffic between the early and later endosomal compartments. *J. Biol. Chem.* 278:34617–34630. doi:10.1074/jbc.M300143200

Hoodless, P.A., T. Haerry, S. Abdollah, M. Stapleton, M.B. O'Connor, L. Attisano, and J.L. Wrana. 1996. MADR1, a MAD-related protein that functions in BMP2 signaling pathways. *Cell*. 85:489–500. doi:10.1016/S0092-8674(00)81250-7

Huntwork, S., and J.T. Littleton. 2007. A complexin fusion clamp regulates spontaneous neurotransmitter release and synaptic growth. *Nat. Neurosci.* 10:1235–1237. doi:10.1038/nn1980

Jia, X.X., M. Gorczyca, and V. Budnik. 1993. Ultrastructure of neuromuscular junctions in *Drosophila*: comparison of wild type and mutants with increased excitability. *J. Neurobiol.* 24:1025–1044. doi:10.1002/neu.480240804

Khodosh, R., A. Augsburger, T.L. Schwarz, and P.A. Garrity. 2006. Bchs, a BEACH domain protein, antagonizes Rab11 in synapse morphogenesis and other developmental events. *Development*. 133:4655–4665. doi:10.1242/dev.02650

Lloyd, T.E., R. Atkinson, M.N. Wu, Y. Zhou, G. Pennetta, and H.J. Bellen. 2002. Hrs regulates endosome membrane invagination and tyrosine kinase receptor signaling in *Drosophila*. *Cell*. 108:261–269. doi:10.1016/S0092-8674(02)00611-6

Macia, E., M. Ehrlich, R. Massol, E. Boucrot, C. Brunner, and T. Kirchhausen. 2006. Dynasore, a cell-permeable inhibitor of dynamin. *Dev. Cell*. 10:839–850. doi:10.1016/j.devcel.2006.04.002

Marqués, G., and B. Zhang. 2006. Retrograde signaling that regulates synaptic development and function at the *Drosophila* neuromuscular junction. *Int. Rev. Neurobiol.* 75:267–285. doi:10.1016/S0074-7742(06)75012-7

McCabe, B.D., G. Marqués, A.P. Haghighi, R.D. Fetter, M.L. Crotty, T.E. Haerry, C.S. Goodman, and M.B. O'Connor. 2003. The BMP homolog Gbb provides a retrograde signal that regulates synaptic growth at the *Drosophila* neuromuscular junction. *Neuron*. 39:241–254. doi:10.1016/S0896-6273(03)00426-4

Mettlen, M., T. Pucadyil, R. Ramachandran, and S.L. Schmid. 2009. Dissecting dynamin's role in clathrin-mediated endocytosis. *Biochem. Soc. Trans.* 37:1022–1026. doi:10.1042/BST0371022

Miech, C., H.U. Pauer, X. He, and T.L. Schwarz. 2008. Presynaptic local signaling by a canonical wingless pathway regulates development of the *Drosophila* neuromuscular junction. *J. Neurosci.* 28:10875–10884. doi:10.1523/JNEUROSCI.0164-08.2008

O'Connor-Giles, K.M., L.L. Ho, and B. Ganetzky. 2008. Nervous wreck interacts with thickveins and the endocytic machinery to attenuate retrograde BMP signaling during synaptic growth. *Neuron*. 58:507–518. doi:10.1016/j.neuron.2008.03.007

Packard, M., E.S. Koo, M. Gorczyca, J. Sharpe, S. Cumberledge, and V. Budnik. 2002. The *Drosophila* Wnt, wingless, provides an essential signal for pre- and postsynaptic differentiation. *Cell*. 111:319–330. doi:10.1016/S0092-8674(02)01047-4

Parnas, D., A.P. Haghighi, R.D. Fetter, S.W. Kim, and C.S. Goodman. 2001. Regulation of postsynaptic structure and protein localization by the Rho-type guanine nucleotide exchange factor dPix. *Neuron*. 32:415–424. doi:10.1016/S0896-6273(01)00485-8

Persson, U., H. Izumi, S. Souchelnytskyi, S. Itoh, S. Grimsby, U. Engström, C.H. Heldin, K. Funa, and P. ten Dijke. 1998. The L45 loop in type I

receptors for TGF-beta family members is a critical determinant in specifying Smad isoform activation. *FEBS Lett.* 434:83–87. doi:10.1016/S0014-5793(98)00954-5

Pylypenko, O., R. Lundmark, E. Rasmuson, S.R. Carlsson, and A. Rak. 2007. The PX-BAR membrane-remodeling unit of sorting nexin 9. *EMBO J.* 26:4788–4800. doi:10.1038/sj.emboj.7601889

Raiborg, C., and H. Stenmark. 2009. The ESCRT machinery in endosomal sorting of ubiquitylated membrane proteins. *Nature*. 458:445–452. doi:10.1038/nature07961

Ramaswami, M., K.S. Krishnan, and R.B. Kelly. 1994. Intermediates in synaptic vesicle recycling revealed by optical imaging of *Drosophila* neuromuscular junctions. *Neuron*. 13:363–375. doi:10.1016/0896-6273(94)90353-0

Rao, Y., Q. Ma, A. Vahedi-Faridi, A. Sundborger, A. Pechstein, D. Puchkov, L. Luo, O. Shupliakov, W. Saenger, and V. Haucke. 2010. Molecular basis for SH3 domain regulation of F-BAR-mediated membrane deformation. *Proc. Natl. Acad. Sci. USA*. 107:8213–8218. doi:10.1073/pnas.1003478107

Rieckhof, G.E., M. Yoshihara, Z. Guan, and J.T. Littleton. 2003. Presynaptic N-type calcium channels regulate synaptic growth. *J. Biol. Chem.* 278:41099–41108. doi:10.1074/jbc.M306417200

Rodal, A.A., R.N. Motola-Barnes, and J.T. Littleton. 2008. Nervous wreck and Cdc42 cooperate to regulate endocytic actin assembly during synaptic growth. *J. Neurosci.* 28:8316–8325. doi:10.1523/JNEUROSCI.2304-08.2008

Rogers, S.L., U. Wiedemann, N. Stuurman, and R.D. Vale. 2003. Molecular requirements for actin-based lamella formation in *Drosophila* S2 cells. *J. Cell Biol.* 162:1079–1088. doi:10.1083/jcb.200303023

Roos, J., and R.B. Kelly. 1998. Dap160, a neural-specific Eps15 homology and multiple SH3 domain-containing protein that interacts with *Drosophila* dynamin. *J. Biol. Chem.* 273:19108–19119. doi:10.1074/jbc.273.30.19108

Roos, J., and R.B. Kelly. 1999. The endocytic machinery in nerve terminals surrounds sites of exocytosis. *Curr. Biol.* 9:1411–1414. doi:10.1016/S0960-9822(00)80087-1

Sadowski, L., I. Pilecka, and M. Miaczynska. 2009. Signaling from endosomes: location makes a difference. *Exp. Cell Res.* 315:1601–1609. doi:10.1016/j.yexcr.2008.09.021

Sone, M., E. Suzuki, M. Hoshino, D. Hou, H. Kuromi, M. Fukata, S. Kuroda, K. Kaibuchi, Y. Nabeshima, and C. Hama. 2000. Synaptic development is controlled in the periactive zones of *Drosophila* synapses. *Development*. 127:4157–4168.

Strigini, M., and S.M. Cohen. 2000. Wingless gradient formation in the *Drosophila* wing. *Curr. Biol.* 10:293–300. doi:10.1016/S0960-9822(00)00378-X

Sweeney, S.T., and G.W. Davis. 2002. Unrestricted synaptic growth in spinster-a late endosomal protein implicated in TGF-beta-mediated synaptic growth regulation. *Neuron*. 36:403–416. doi:10.1016/S0896-6273(02)01014-0

Van Hoof, D., K.W. Rodenburg, and D.J. Van der Horst. 2005. Receptor-mediated endocytosis and intracellular trafficking of lipoproteins and transferrin in insect cells. *Insect Biochem. Mol. Biol.* 35:117–128. doi:10.1016/j.ibmb.2004.09.009

Verstreken, P., T. Ohyama, and H.J. Bellen. 2008. FM 1-43 labeling of synaptic vesicle pools at the *Drosophila* neuromuscular junction. *Methods Mol. Biol.* 440:349–369. doi:10.1007/978-1-59745-178-9_26

Wang, Q., H.Y. Kaan, R.N. Hooda, S.L. Goh, and H. Sondermann. 2008a. Structure and plasticity of Endophilin and Sorting Nexin 9. *Structure*. 16:1574–1587. doi:10.1016/j.str.2008.07.016

Wang, X., W.R. Shaw, H.T. Tsang, E. Reid, and C.J. O'Kane. 2007. *Drosophila* spichthyin inhibits BMP signaling and regulates synaptic growth and axonal microtubules. *Nat. Neurosci.* 10:177–185. doi:10.1038/nn1841

Wang, Z., J.G. Edwards, N. Riley, D.W.J. Provance Jr., R. Karcher, X.D. Li, I.G. Davison, M. Ikebe, J.A. Mercer, J.A. Kauer, and M.D. Ehlers. 2008b. Myosin Vb mobilizes recycling endosomes and AMPA receptors for postsynaptic plasticity. *Cell*. 135:535–548. doi:10.1016/j.cell.2008.09.057

Wieser, R., J.L. Wrana, and J. Massagué. 1995. GS domain mutations that constitutively activate T beta R-I, the downstream signaling component in the TGF-beta receptor complex. *EMBO J.* 14:2199–2208.

Wucherpfennig, T., M. Wilsch-Bräuninger, and M. González-Gaitán. 2003. Role of *Drosophila* Rab5 during endosomal trafficking at the synapse and evoked neurotransmitter release. *J. Cell Biol.* 161:609–624. doi:10.1083/jcb.200211087

Yarar, D., M.C. Surka, M.C. Leonard, and S.L. Schmid. 2008. SNX9 activities are regulated by multiple phosphoinositides through both PX and BAR domains. *Traffic*. 9:133–146. doi:10.1111/j.1600-0854.2007.00675.x

Yoshihara, M., B. Adolfsen, K.T. Galle, and J.T. Littleton. 2005. Retrograde signaling by Syt 4 induces presynaptic release and synapse-specific growth. *Science*. 310:858–863. doi:10.1126/science.1117541

Zinsmaier, K.E., K.K. Eberle, E. Buchner, N. Walter, and S. Benzer. 1994. Paralysis and early death in cysteine string protein mutants of *Drosophila*. *Science*. 263:977–980. doi:10.1126/science.8310297

Published April 4, 2011

Rodal et al., http://www.jcb.org/cgi/content/full/jcb.201009052/DC1

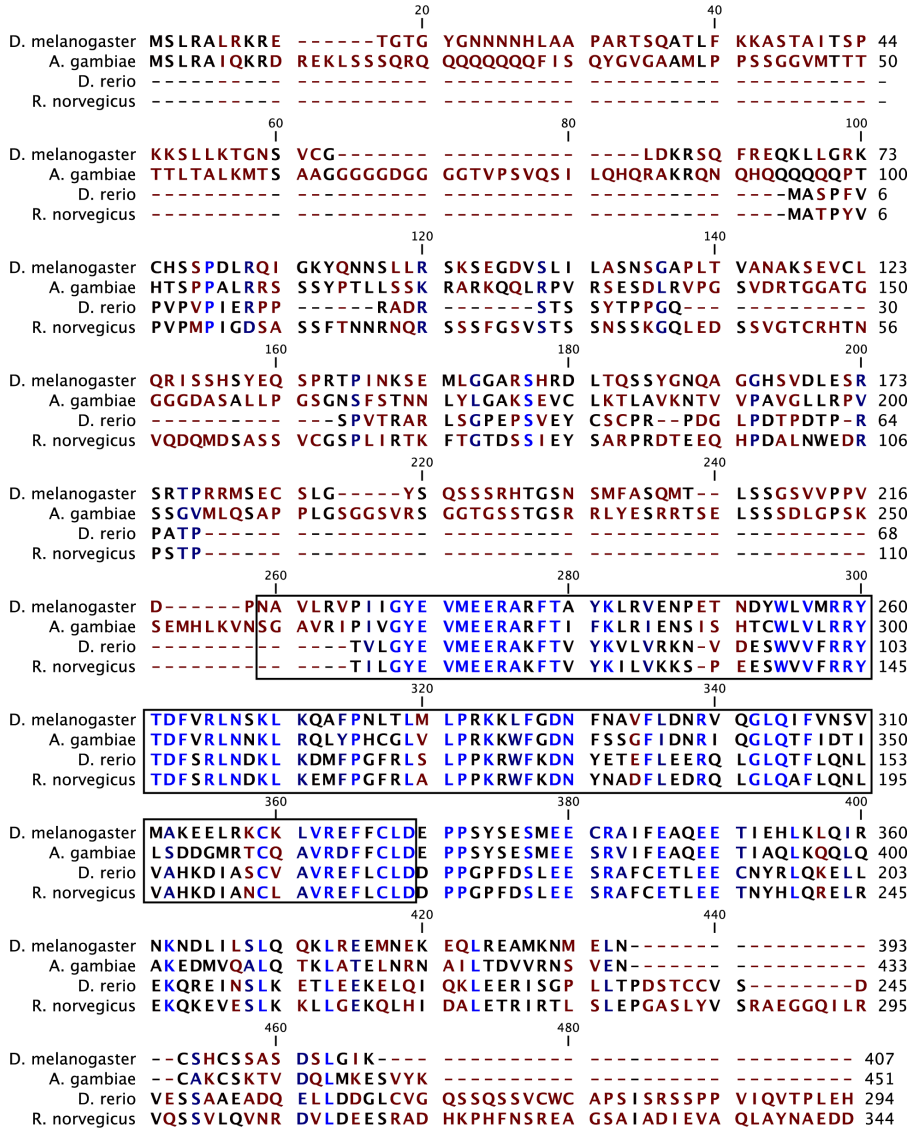

Figure S1. **Alignment of SNX16 homologues (associated with Fig. 1).** SNX16 homologues were aligned using ClustalW2 (Larkin et al., 2007). NCBI Protein database accession numbers are XP_001688026 (*A. gambiae*), NP_991228 (*D. rerio*), and AAG25677 (*R. norvegicus*) and the boxed area indicates the PX domain. Blue indicates residues that are identical between species, and red indicates residues that are similar between species.

Published April 4, 2011

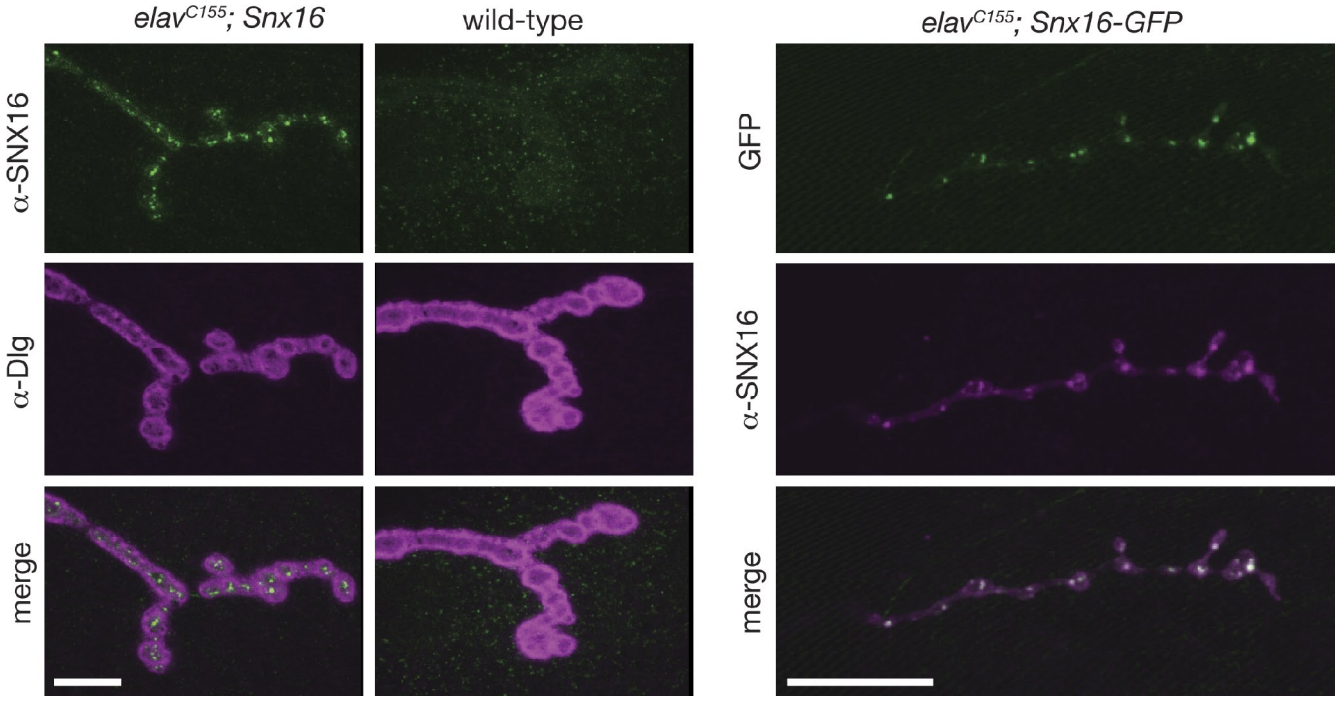

Figure S2. **Specificity of α-SNX16 antibodies (associated with Fig. 2).** Third instar larvae of the indicated genotypes were stained with the indicated antibodies and imaged at muscle 4, segment A2 or A3. Left and middle images were imaged under identical settings. Bars, 10 µm.

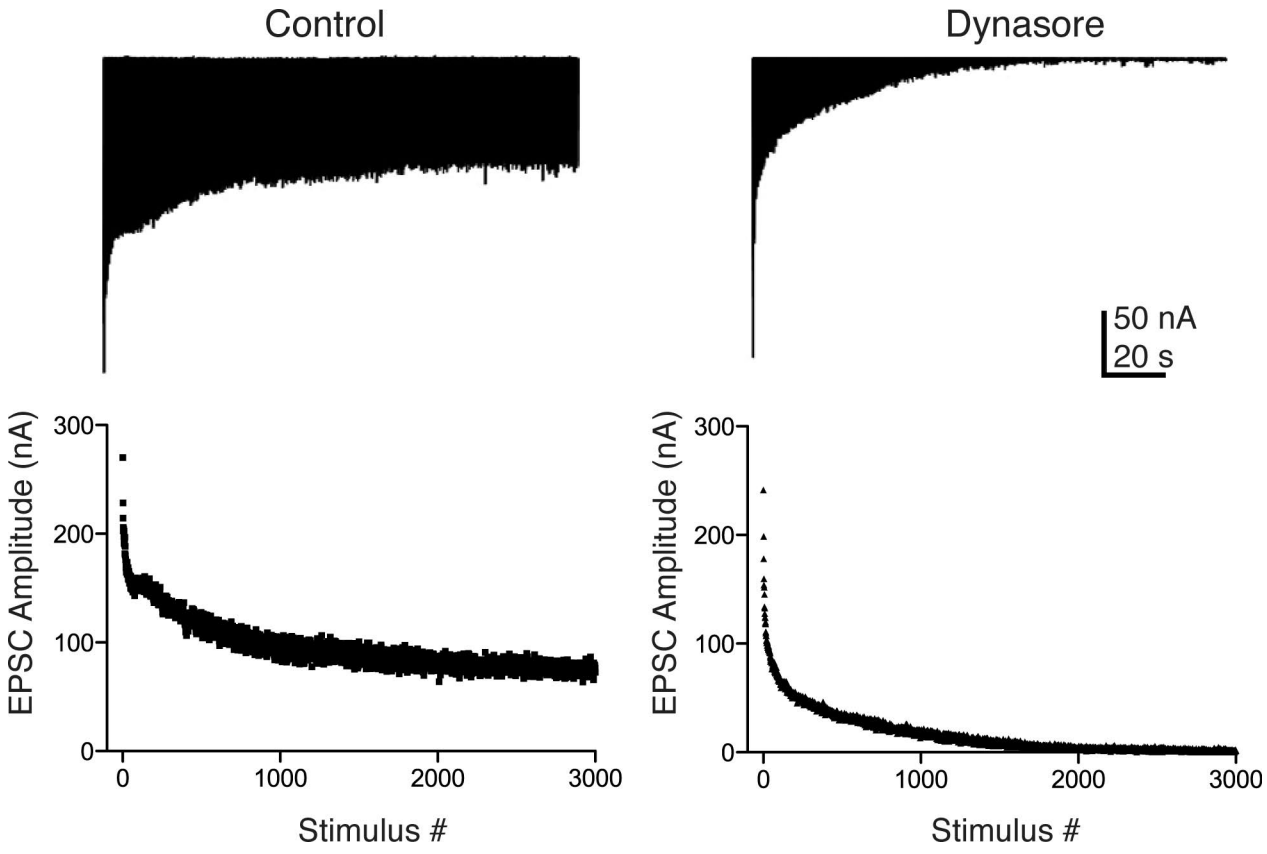

Figure S3. **Voltage clamp recordings at the NMJ of third instar larvae (associated with Fig. 4).** Excitatory postsynaptic currents were elicited by stimulating the nerve at 20 Hz in DMSO (top left)- or dynasore-treated synapses (top right). The postsynaptic current traces represent continuous tetanizing stimulus trains. Bottom shows quantification of the mean EPSCs in control and treated synapses (n = 4 animals).

Published April 4, 2011

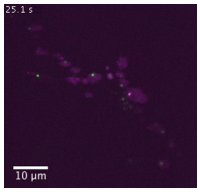

Video 1. **Nwk-mRFP and SNX16-GFP puncta transiently associate in synaptic boutons (associated with Fig. 4).** Animal 1. Third instar NMJs from larvae expressing *Snx16*-GFP and *nwk*-mRFP (under the control of the panneuronal driver *elav*^{C155}) were imaged at one z stack/2–2.5 s using a spinning-disk confocal microscope (Marianis; 3i People, Inc.). Time-lapse series at 10× live speed shows maximum intensity projections of confocal z series.

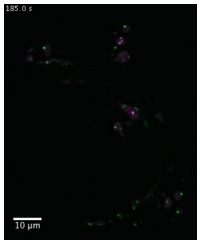

Video 2. **Nwk-mRFP and SNX16-GFP puncta transiently associate in synaptic boutons (associated with Fig. 4).** Animal 2. Third instar NMJs from larvae expressing *Snx16*-GFP and *nwk*-mRFP (under the control of the panneuronal driver *elav*^{C155}) were imaged at one z stack/2–2.5 s using a spinning-disk confocal microscope (Marianis). Time-lapse series at 10× live speed shows maximum intensity projections of confocal z series.

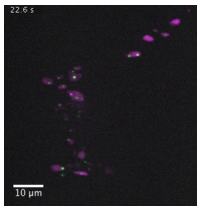

Video 3. **Nwk-mRFP and SNX16-GFP puncta transiently associate in synaptic boutons (associated with Fig. 4).** Animal 3. Third instar NMJs from larvae expressing *Snx16*-GFP and *nwk*-mRFP (under the control of the panneuronal driver *elav*^{C155}) were imaged at one z stack/2–2.5 s using a spinning-disk confocal microscope (Marianis). Time-lapse series at 10× live speed shows maximum intensity projections of confocal z series.

Reference

Larkin, M.A., G. Blackshields, N.P. Brown, R. Chenna, P.A. McGettigan, H. McWilliam, F. Valentin, I.M. Wallace, A. Wilm, R. Lopez, et al. 2007. Clustal W and Clustal X version 2.0. *Bioinformatics*. 23:2947–2948. doi:10.1093/bioinformatics/btm404